Progress in Neurobiology 223 (2023) 102386

Contents lists available at ScienceDirect

Progress in Neurobiology

journal homepage: www.elsevier.com/locate/pneurobio

Tau promotes oxidative stress-associated cycling neurons in S phase as a pro-survival mechanism: Possible implication for Alzheimer's disease

Marine Denechaud [a,1], Sarah Geurs [c,d,1], Thomas Comptdaer [a], Séverine Bégard [a], Alejandro Garcia-Núñez [a], Louis-Adrien Pechereau [a], Thomas Bouillet [a], Yannick Vermeiren [e], Peter P. De Deyn [e,f], Romain Perbet [a], Vincent Deramecourt [a,h], Claude-Alain Maurage [a,h], Michiel Vanderhaegen [d], Sebastiaan Vanuytven [d], Bruno Lefebvre [a], Elke Bogaert [c], Nicole Déglon [g], Thierry Voet [d,i], Morvane Colin [a], Luc Buée [a], Bart Dermaut [b,c,1], Marie-Christine Galas [a,*,1]

[a] University of Lille, Inserm, CHU Lille, CNRS, LilNCog - Lille Neuroscience & Cognition, F-59000 Lille, France
[b] Center for Medical Genetics, Ghent University Hospital, 9000 Ghent, Belgium
[c] Department of Biomolecular Medicine, Faculty of Medicine and Health Sciences, Ghent University, 9000 Ghent, Belgium
[d] Department of Human Genetics, University of Leuven (KU Leuven), 3000 Leuven, Belgium
[e] Laboratory of Neurochemistry and Behavior, and Biobank, Institute Born-Bunge, University of Antwerp, Universiteitsplein 1, BE-2610 Antwerpen, Belgium
[f] Department of Neurology and Memory Clinic, Hospital Network Antwerp (ZNA) Middelheim and Hoge Beuken, eindendreef 1, 2020 Antwerpen, Belgium
[g] Lausanne University Hospital (CHUV) and University of Lausanne, Neuroscience Research Center (CRN), Laboratory of Cellular and Molecular Neurotherapies, 1011 Lausanne, Switzerland
[h] Department of Pathological Anatomy, University of Lille, CHU Lille, Lille, France
[i] KU Leuven, Institute for Single Cell Omics (LISCO), KU Leuven, 3000 Leuven, Belgium

ARTICLE INFO

Keywords:
Alzheimer's disease
Tau
Oxidative stress
Cell cycle
S phase
Pro-survival

ABSTRACT

Multiple lines of evidence have linked oxidative stress, tau pathology and neuronal cell cycle re-activation to Alzheimer's disease (AD). While a prevailing idea is that oxidative stress-induced neuronal cell cycle reactivation acts as an upstream trigger for pathological tau phosphorylation, others have identified tau as an inducer of cell cycle abnormalities in both mitotic and postmitotic conditions. In addition, nuclear hypophosphorylated tau has been identified as a key player in the DNA damage response to oxidative stress. Whether and to what extent these observations are causally linked remains unclear. Using immunofluorescence, fluorescence-activated nucleus sorting and single-nucleus sequencing, we report an oxidative stress-associated accumulation of nuclear hypophosphorylated tau in a subpopulation of cycling neurons confined in S phase in AD brains, near amyloid plaques. Tau downregulation in murine neurons revealed an essential role for tau to promote cell cycle progression to S phase and prevent apoptosis in response to oxidative stress. Our results suggest that tau holds oxidative stress-associated cycling neurons in S phase to escape cell death. Together, this study proposes a tau-dependent

Abbreviations: clsm, confocal laser-scanning microscope/microscopy; DDR, DNA damage response; DSB, double strand break; FANS, fluorescence-activated nucleus sorting; γH2AX/gH2AX, phosphorylated form of Histone H2AX (PSer139-H2AX); ntau+, nuclear tau positive; 8oxoG, 8-oxo-7,8-dihydroguanine; PCNA, proliferating cell nuclear antigen; PH3, phosphorylated form of Histone H3 (PSer10); PCF, piecewise constant fitting; scWGS, single-cell whole genome sequencing; sh, short hairpin.

* Corresponding author.
E-mail addresses: marine.denechaud@inserm.fr (M. Denechaud), sarah.geurs@kuleuven.be (S. Geurs), thomas.comptdaer@inserm.fr (T. Comptdaer), severine.begard@inserm.fr (S. Bégard), hpayns@gmail.com (A. Garcia-Núñez), louisadrien.pechereau@gmail.com (L.-A. Pechereau), thomas.bouillet@inserm.fr (T. Bouillet), yannick.vermeiren@uantwerpen.be (Y. Vermeiren), peter.dedeyn@uantwerpen.be (P.P. De Deyn), RPERBET@mgh.harvard.edu (R. Perbet), Vincent.DERAMECOURT@CHRU-LILLE.FR (V. Deramecourt), Claude-Alain.MAURAGE@CHRU-LILLE.FR (C.-A. Maurage), michiel.vanderhaeghen@kuleuven.be (M. Vanderhaegen), sebastiaan.vanuytven@kuleuven.be (S. Vanuytven), bruno.lefebvre@inserm.fr (B. Lefebvre), Elke.Bogaert@UGent.be (E. Bogaert), nicole.deglon@chuv.ch (N. Déglon), thierry.voet@kuleuven.be (T. Voet), morvane.colin@inserm.fr (M. Colin), luc.buee@inserm.fr (L. Buée), bart.dermaut@ugent.be (B. Dermaut), marie-christine.galas@inserm.fr (M.-C. Galas).
[1] equal contribution

https://doi.org/10.1016/j.pneurobio.2022.102386
Received 23 May 2022; Received in revised form 24 November 2022; Accepted 2 December 2022
Available online 6 December 2022

protective effect of neuronal cell cycle reactivation in AD brains and challenges the current view that the neuronal cell cycle is an early mediator of tau pathology.

1. Introduction

Neurons, although defined as post mitotic cells, are able to re-activate the cell cycle machinery in response to various stresses including oxidative DNA damage (Kagias et al., 2012). Neurons that re-enter the cell cycle proceed from G0 to G1, until they reach the G1/S checkpoint. At this point they either undergo re-differentiation or irreversibly move further through the cell cycle ultimately resulting in apoptosis (Busser et al., 1998; Herrup et al., 2004; Aranda-Anzaldo et al., 2017). In neurotypical human brains, however, a small population of differentiated neurons do re-initiate the cell cycle and pass the G1/S checkpoint but escape apoptosis. These neurons have hence partially or fully replicated their genome (Mosch et al., 2007; López-Sánchez et al., 2017) and, surprisingly, survive for years with this altered DNA content, suggesting that pro-survival mechanisms are activated to prevent cell death. Interestingly, state-of-the-art single-cell whole genome sequencing (scWGS) studies have indeed confirmed the presence of DNA content alterations and somatic structural genome variation in cerebral neurons (McConnell et al., 2013; Cai et al., 2014; Lodato et al., 2015). Full-chromosome aneuploidies were reported in 2.7 % of neurons from neurotypical post-mortem human brain, while 5–41 % of the neurons are estimated to carry at least one mega-base scale copy number variation (McConnell et al., 2013). Although the biological relevance of DNA content variation in the neurotypical brain remains largely enigmatic, over the last three decades, links with neurodegeneration associated with tau pathology have been put forward in the literature. Neurons with altered DNA content were identified in the cortex of AD patients with increased observation in regions specifically vulnerable to neurodegeneration (Bajic et al., 2015; López-Sánchez et al., 2017). An increased DNA content in mature, post-mitotic neurons can have originated during neurogenesis due to mitotic errors or can result from aberrant cell cycle re-activation with subsequent DNA replication (Arendt et al., 2009; Arendt, 2012; Potter et al., 2019). Supporting the mitotic errors scenario, several studies in *Drosophila* and cell culture primary tauopathy models show a toxic role for tau during mitosis leading to abnormal monopolar spindles and increased numbers of aneuploid neuronal cells (Bougé et al., 2016; Malmanche et al., 2017; Martellucci et al., 2021). Moreover, aneuploidies are found in peripheral blood cells and primary fibroblast cultures from patients who carry known tau mutations causing frontotemporal dementia (Rossi et al., 2008, 2013). However, one low-coverage scWGS study did not detect an increased level of single chromosome aneuploidies in AD donor brain-derived neurons (van den Bos et al., 2016). On the other hand, an increased number of neuronal cell cycle events has been observed in brains of patients at early stages of Alzheimer's disease (AD) or patients with mild cognitive impairment (Arendt, 2000; Yang et al., 2003; Hoozemans et al., 2002; Pei et al., 2002; Johansson et al., 2003; Zhu et al., 2004; Bonda et al., 2009; Stone et al., 2011; López-Sánchez et al., 2017; Gao et al., 2018). As increased numbers of cell cycle events as well as increased DNA content are observed in AD, it is reasonable to speculate that both phenomena are causally linked. Furthermore, the fact that these abnormalities appear in the early stages of disease, suggests a crucial primary role for this process in AD pathogenesis (López-Sánchez et al., 2017; Shepherd, 2018).

In AD brains, cell cycle markers are upregulated in neurons with hyperphosphorylated (hyperP) cytoplasmic tau (Arendt et al., 1995; Nagy et al., 1997; Schindowski et al., 2008; Huang et al., 2019). Likewise, disease-associated tau hyperphosphorylation is observed in mitotic neuroblastoma, non-neuronal proliferative cells and *Xenopus laevis* oocytes (Illenberger et al., 1998; Delobel et al., 2002; Flores-Rodríguez et al., 2019) leading to the hypothesis that re-entry of the cell cycle could lead to hyperphosphorylation of tau. Nevertheless, the nuclear expression of proliferation markers in AD brains does not systematically overlap with the presence of phosphorylated forms of tau, which further supports the idea that neuronal cell cycle reactivation could act as an upstream trigger of tau pathology (Stone et al., 2011; Hradek et al., 2015). However, various studies, attempting to determine whether tau phosphorylation is a cause or rather a result of cell cycle reactivation, provided evidence for both scenarios (Andorfer et al., 2005; Khurana et al., 2006; McShea et al., 2007; Park et al., 2007; Schindowski et al., 2008).

Interestingly, oxidative stress, with its increased production of reactive oxygen species (ROS), and genotoxic factors have been shown to trigger cell cycle re-entry in differentiated neurons via the DNA damage response (DDR) (Kruman et al., 2004; Cioffi et al., 2019; Shanbhag et al., 2019). Moreover, we and others have demonstrated that inducers of DNA damage such as oxidative stress can trigger an increase of hypophosphorylated (hypoP) tau in neuronal and non-neuronal nuclei (Sultan et al., 2011, Ulrich et al., 2018; Portillo et al., 2021). In addition, it has been shown that nuclear tau is a key factor in the DDR in neurons and is pivotal to preserve DNA integrity in physiological and stress condition (Sultan et al., 2011, Violet et al., 2014; Mansuroglu et al., 2016; Bou Samra et al., 2017).

Links between oxidative stress, nuclear tau, tau pathology and neuronal cell cycle re-activation are strongly suggested in the literature. However, the precise causal relationship remains unclear and under-explored. We therefore designed a study to further explore these questions in human AD brain cortex. Our research revealed an oxidative stress-associated nuclear accumulation of hypoP tau in a subpopulation of cycling neurons (ntau$^+$ cycling neurons) that are likely blocked in S-phase and which can specifically be found in the vicinity of amyloid plaques. Further experiments in differentiated cortical neurons revealed an essential role for tau to promote neuronal cell cycle progression to S-phase and prevent apoptosis in response to oxidative stress. Our observations suggest that the combination of increased nuclear tau and the cell cycle reactivation in neurons prevents oxidative stress-induced deleterious effects and promotes cell survival at early stages of AD. Our results challenge the current view of neuronal cell cycle activation as an early driver of AD pathogenesis and rather suggest a pro-survival role for tau-mediated cell cycle progression.

2. Materials and methods

2.1. Tissue collection

Adult human brain samples were obtained from the Lille Neurobank (Lille, France) and from the Neurobiobank of the Institute Born-Bunge (NBB-IBB; FAGG enlisted registration number BB190113) (University of Antwerp, Belgium). Human brains from the Lille Neurobank were given to the French Research Ministry by the Lille Regional Hospital (CHRU-Lille) on August 14, 2008 under the reference DC- 2000–642. Frontal and temporal cortex sections from human non-demented control (C) and Braak VI Alzheimer brains (AD) associated to amyloid pathology (Thal score 2–5) from the Lille Neurobank (C n = 4; AD n = 5) were used for immunofluorescence analysis. Frozen frontal cortex tissue blocks from human non-demented control (C) and Braak V-VI Alzheimer brains (AD) associated to amyloid pathology (Thal score 1–5) from the Lille Neurobank and the Neurobiobank of the Institute Born-Bunge were used for FANS analysis (C n = 6; AD n = 9), immunofluorescence analysis of sorted nuclei (C n = 5; AD n = 5) and single-nucleus genome sequencing (C n = 1; AD n = 2). (Table 1).

Given the size of the human cortex, the blocks can come from

Table 1
Braak and Thal scores, region, age, gender, and post mortem interval of the brains.

	Braak score	Thal score	Tissue	Age	Sex	PMIa (hours)
C#1	0	0	Frontal Cortex	74	M	48
C#2	II	0	Frontal Cortex	72	F	72
C#3	0	0	Frontal Cortex	62	M	60
C#4	I	0	Frontal Cortex	90	F	16
C#5	I	0	Frontal Cortex	69	M	21
C#6	0	0	Frontal Cortex	64	F	30
C#7	I	0	Frontal Cortex	74	M	46
AD#1	VI	5	Frontal Cortex	76	F	22
AD#2	VI	5	Frontal Cortex	67	M	36
AD#3	VI	5	Temporal Cortex	61	M	23
AD#4	V-VI	2	Temporal Cortex	94	M	6
AD#5	VI	5	Temporal Cortex	73	F	5,5
AD#6	VI	4	Frontal Cortex	63	M	20
AD#7	VI	4–5	Frontal Cortex	63	M	21
AD#8	VI	5	Frontal Cortex	65	M	36
AD#9	VI	4	Frontal Cortex	68	F	6
AD#10	VI	4	Frontal Cortex	68	M	6
AD#11	VI	4	Frontal Cortex	62	M	6
AD#12	V	1	Frontal Cortex	69	F	60
AD#13	VI	5	Frontal Cortex	49	M	7
AD#14	VI	4	Frontal Cortex	67	M	9,5
C#8	NA	NA	Frontal Cortex	87	M	7,5
C#9	NA	NA	Frontal Cortex	78	M	6
C#10	0	0	Frontal Cortex	79	F	7
C#11	I	NA	Frontal Cortex	73	F	1,5
C#12	I-II	I	Frontal Cortex	90	F	1,5
C#13	II-III	3	Frontal Cortex	108	F	7

Human brains used for immunofluorescence analysis
Lille Neurobank
Human brains used for FANS analysis
Lille Neurobank
Neurobiobank of the Institute Born-Bunge[a]PMI: Post mortem interval
Anonymized data
Presence of pathogenic clinical mutation
AD#11 – PSEN2 p.Arg71Trp (pathogenic nature unclear); AD#13 – PSEN1 p. Glu120Asp (pathogenic); AD#14 – PSEN2 p.Ser130Leu (pathogenic nature unclear)

different areas within frontal and temporal cortex. Therefore, it cannot be completely excluded that some of the variability obtained in the results is related to regional differences.

2.2. Primary neuronal culture

Mouse primary cortical neurons were prepared from 14- to 15-day old C57BL/6 mouse embryos as followed. Briefly, brain and meninges were removed. Cortex was carefully dissected out and mechanically dissociated in culture medium (Leibovitz's L15, Life Technologies, 21083027) supplemented with 30 mM glucose, by triturating with a polished Pasteur pipette. Once dissociated and after blue trypan counting, cells were plated at a density of 1600 cells/mm2 in poly-D-lysine (0.1 mg/ml, Sigma-Aldrich, P0899) and laminin (20 μg/ml, Sigma-Aldrich, L2020) coated in 24 wells plates. For dissociation, plating and maintenance, we used Neurobasal medium (Life Technologies, 21103049) supplemented with 1 % B27 (Life Technologies, 17504044) containing 200 mM glutamine (Life Technologies, 25030024) and 1 % antibiotic-antimycotic agent (Life Technologies, 15240096). Medium was replenished weekly from 14 DIV to 24 DIV and never more than 20 % of total volume.

Oxidative stress was induced by 1 H treatment with 1 mM hydrogen peroxide (H_2O_2) (Sigma, H1009) or tert-Butyl hydrogen peroxide (tBut-H_2O_2) (Acros Organics, AC180342500).

For experiments in which DNA replication was monitored, BrdU (Sigma, B9285) was added to medium at 10 μM at the same time as H_2O_2.

2.3. Immunofluorescence of brain sections and primary neuronal cultures

Immunofluorescence on brain sections was performed as described previously (Zheng et al., 2020). Briefly, coronal (5 μM) brain slices were deparaffinized and unmasked using citrate buffer (12 mM citric acid, 38 mM Sodium phosphate dibasic, pH 6) for 8 min in a pressure tank.

For Abeta labeling, the slices were unmasked using formic acid (80 % in water) for 3 min followed by 6 water rinces before the citrate buffer treatment. The slices were submerged for 1 h in 1 % horse serum (Vector Laboratories #S-2000), and the primary antibodies were incubated overnight at 4 °C in the presence of PBS-0.2 % Triton.

Primary antibodies were revealed via secondary antibodies coupled to Alexa 488, 568 or 647 (Life Technologies). The sections were counterstained with 4′,6-Diamidino-2-phenylindole (DAPI) and mounted with fluorescence mounting medium (Agilent Dako #S3023).

Immunofluorescence on primary neuronal cultures was performed as described previously (Galas et al., 2006).

The following antibodies were used: AT8 (PSer202/Thr205tau; ThermoFisher Scientific MN1020), AD2 (PSer396–404tau) (Buée-Scherrer et al., 1996), AT270 (PThr181tau; ThermoFisher Scientific MN1050), PSer262tau (ThermoFisher Scientific 44750G), Tau1 (unPSer195, 198, 199, and 202tau; Sigma Aldrich MAB3420)(AT8, AD2, AT270, PSer262tau, Tau1 are phospho-dependent antibodies which are present from the early to late stages of tau pathology), 4E4 (phosphorylation-independent antibody against tau C-terminal sequence, used for IF) (Nobuhara et al., 2017), 9H12 (laboratory-made phosphorylation-independent antibody against the 162–175 central region of tau, used for WB), 8oxoG (Novus biologicals NB600–1508), γH2AX (Sigma Aldrich 05–636), Ki67 (abcam ab16667 and R&D systems #AF7617), cyclin D1 (ThermoFisher Scientific PA5–16607), PCNA (Genetex GTX100539), cyclin A (Santa Cruz Biotechnology, sc 596), cyclin B1 (Genetex GTX100911), Phospho Histone H3 (Sigma Aldrich 06–570); cleaved caspase 3 (Sigma Aldrich C8487), NeuN (Sigma Aldrich, ABN90), beta amyloid (Abeta) (Covance SIG-39240; Bio--Legends SIG-39340), GFP (Invitrogen, A11122), beta actin (Sigma, A5441). DAPI and Hoechst were used as a chromatin counterstain. Nuclear (based on DAPI or Hoechst detection) labeling of cells were quantified using the FIDJI macro application of ImageJ (confocal microscopy platform, PBSL, UAR2014/US41, Lille). Fluorescence from human brain sections (C n = 4, AD n = 5) and primary neuronal cultures (n = 10) was acquired using an LSM 710 confocal laser-scanning microscope (clsm) (Carl Zeiss). The confocal microscope was equipped with a 488-nm Argon laser, 561-nm diode-pumped solid-state laser, and a 405-nm ultraviolet laser. The images were acquired using an oil 63X Plan-APOCHROMAT objective (1.4 NA). All recordings were performed using the appropriate sampling frequency (16 bits, 1024–1024 images, and a line average of 4). Serial sections from the three-dimensional reconstruction (IMARIS software) were acquired using Z-steps of 0.2 μm. For each section, nuclear (based on DAPI detection) fluorescence of cells was quantified using the FIDJI macro application of ImageJ (confocal microscopy platform, PBSL, UAR2014/US41, Lille). Quantification corresponds to the z stack of serial confocal sections covering the entire thickness of the brain section. The quantification shows the mean of nuclear fluorescence values per individual.

2.4. Plasmid construction

The shGFP (AAGCTGACCCTGAAGTTCATTCAAGAGATGAACTTCA GGGTCAGCTTTTT; passenger-loop- guide strand) was cloned in the pCCL transfer plasmid (Dull et al., 1998) and used as control (shctrl) in silencing experiments. The H1-shtau (CAGGAAATGACGAGAA-GAAACTTCCTGTCATTTCTTCTCGTCATTTCCTGTTTTTT) was first cloned into the Gateway Entry pENTR/D/TOPO vector (Invitrogen, St

Aubin, France) using TOPO TA cloning methodology. The Gateway LR Clonase (Invitrogen) was used to catalyze the in vitro recombination between the Gateway Entry pENTR/D/TOPO-H1-shtau vector and the lentiviral destination plasmid (SIN-cPPT-PGK-GFP-WPRE-LTR-Gateway). The final vector SIN-cPPT-PGK-GFP-WPRE-LTR-shtau was verified by sequencing.

2.5. Production and assay of recombinant lentiviral vectors

Lentiviral vectors (LVs) were amplified as previously described (Hottinger et al., 2000). HEK293T cells (4×10^6) were plated on 10-cm plates and transfected the following day with 13 μg of LV-H1-shGFP (hereafter called LV-shctrl) or LV-PGK-tomato-H1-shGFP (hereafter called LV-tomato-shctrl), 13 μg of pCMVΔR8.92(Tat$^+$), 3 μg of pRSV-Rev, and 3.75 μg of pMD 0.2 G (VSV-G envelope) using the calcium phosphate DNA precipitation procedure. LV-shtau was produced in a similar manner but replacing pCMVΔR8.92 (Tat+) with pMD-Lg_p-RRE (tat). Four to six hours later, the medium was removed and replaced by fresh medium. Forty-eight hours later, the supernatant was collected and filtered. High-titer stocks were obtained by two successive ultracentrifugation steps at 19,000 rpm (SW 32Ti and SW 60Ti rotors; Beckman Coulter, Villepinte, France) at 4 °C. The pellet was resuspended in PBS with 1% bovine serum albumin and stored frozen at − 80 °C until use.

Viral titer. Viral concentrations were determined using independent assays as follows: (i) The physical titer was quantified using ELISA for the HIV-1 p24 antigen (Gentaur BVBA, Paris, France). The p24 protein is a lentiviral capsid protein that is commonly used in ELISA assays to determine the physical titer of lentiviral batches per milliliter. The LV-shctrl and LV-tomato-shctrl are a gift of Nicole Déglon (Lausanne University).

2.6. Infection of primary neuronal cultures with lentiviral vectors

At DIV7, primary neuronal cultures (n = 7) cultured in 24 wells plates were infected with 50 ng of LVs containing either an shRNA directed against tau (shtau) or a shRNA directed against the green fluorescent protein (shctrl). After 6 h, the infection medium was removed and replaced by conditioned medium. Primary neuronal cultures were then harvested at 37 °C in 5 % CO_2 atmosphere until DIV24. At DIV24, neurons were treated with 1 mM of H_2O_2 (H1009, Sigma) or with PBS (Gibco) for 1 h. Primary neuronal cultures are then washed with 37 °C PBS and fixed using 4 % paraformaldehyde. Two to five different cultures were used to test the effect of LV infection.

2.7. Statistics for immunofluorescence analysis

The Shapiro–Wilk test of normality (GraphPad Prism 7) was used to test if the data were normally distributed. Two-tailed, unpaired Student's t-test (GraphPad Prism 7) was used for statistical analysis of immunofluorescence in human brains. Each biological replicate corresponds to one brain. Mann Whitney U test (GraphPad Prism 7) was used for statistical analysis of immunofluorescence in murine primary neuronal cultures. Each biological replicate corresponds to one cell. For each quantification, analyzed cells are coming from two to five different cultures. The number of biological replicates is indicated in the legends. The experimenters were not blinded. Data are presented as mean ± SEM, *P < 0.05; **P < 0.01; ***P < 0.001; ****P < 0.0001. The associations between nuclear proteins in human post mortem brain and in murine primary neuronal cultures were tested using Pearson correlations and linear regression analysis (GraphPad Prism 7). Each biological replicate corresponds to one cell.

2.8. Single nucleus suspension generation from frozen post-mortem human brain

Neuronal nuclear suspensions from post-mortem frontal cortex tissue blocks were prepared according to Swiech et al. with in-house modifications (Swiech et al., 2015). In more detail, 2 mm^3 frozen frontal cortex tissue blocks were transferred to glass vessels (Fisher scientific 10075911) containing 1 ml of homogenization buffer (HB) (320 mM sucrose, 5 mM $CaCl_2$, 3 mM $Mg(Ac)_2$, 10 mM Tris-HCl pH 7.8, 0.1 mM EDTA, 0.1% NP40, 0.1 mM PMSF, 1 mM beta-mercaptoethanol). Tissue was thawed and homogenized on ice with 35 manual gentle strokes of a plain plunger head (Fisher scientific 10709382). Homogenate was transferred to recipient containing 2.65 ml gradient medium (GM) (5 mM $CaCl_2$, 50% Optiprep™ (Stemcell Technologies), 3 mM $Mg(Ac)_2$, 10 mM Tris HCl pH 7.8, 0.1 mM PMSF, 1 mM beta-mercaptoethanol) and glass vessel was washed with 1.65 ml HB. HB and GM were mixed by inversion and layered on top 5.25 ml of a 29 % Optiprep-sucrose cushion (150 mM KCl, 30 mM $MgCl_2$, 60 mM Tris HCl pH 8, 250 mM sucrose, 29 % Optiprep™) in Open-Top Thinwall Ultra-Clear Tubes (Beckman coulter 344059) for ultracentrifugation at 7700 rpm for 30 min at 4 °C in a SW41-Ti swinging bucket rotor (Beckman Coulter 331362). Supernatant was removed and nuclei pellet was resuspended in PBS+ 0.04%BSA to reach a concentration of approximately 1 million nuclei per ml. Nuclei suspension was filtered through 35 μm mesh and stained with 1 μg/ml anti-NeuN-568 (Abcam ab207282) and 3 μM DAPI.

2.9. Fluorescence activated nucleus sorting (FANS) and analysis

Nuclei suspensions derived from human post-mortem control and AD brains were subjected to FANS on the SH800S Cell Sorter (Sony). Nuclei were discriminated from debris based on side scatter pulse area (SSC-A) and forward scatter pulse area (FSC-A). Subsequently, a strict doublet discrimination was performed based on the pulse width of the forward scatter (FSC-W) versus the pulse height of the forward scatter (FSC-H). Remaining debris was gated against by selecting only DAPI-positive nuclei. Neuronal nuclei were detected based on NeuN expression. Neuronal nuclei with an increased DNA content were visualized on a linear DAPI pulse area (DAPI-A) histogram and selected for single nucleus sorting onto cover slips pre-coated with Poly-D-lysine/Laminin (Corning 354087) in 24-well plates for immunohistochemistry or into 96-well plates containing 2.5 μL RLT+ buffer (Qiagen) per well for single-cell genome sequencing. The percentage of cycling neurons per brain was determined in FlowJo10.8 as the fraction of single neuronal nuclei with a DAPI-A signal higher than two standard deviations from the mean DAPI-A signal. Recordings including less than 700 events were excluded from the analysis. Unpaired two-Samples Wilcoxon statistical testing was performed in R (version 1.1.447) to determine the significance level of the difference between the number of nuclei with increased DNA content in AD versus control brains.

2.10. Immunofluorescence of single nuclei

A 24-wells plate, containing nuclei sorted onto pre-coated cover slips, was centrifuged at 1000 g for 5 min at 4 °C. Nuclei were fixed with 10% paraformaldehyde for 10 min at room temperature (RT). Coverslips were rinsed 3 times with 1x PBS for 10 min. Nuclei fixed onto coverslips were kept in 1xPBS at 4 °C for maximum 1 week. Coverslip was rinsed 2 times with 1x PBS for 10 min at RT when kept at 4 °C. Nuclei were permeabilized with 0.2 % Triton X-100 for 10 min at RT and rinsed 3 times with 1x PBS for 5 min at RT. 2 % normal donkey serum was used for blocking for 10 min at RT. 1:200 mouse Tau1 primary antibody was administered to the nuclei and incubated overnight at 4 °C in the dark. Coverslips were rinsed 3 times with 1x PBS for 10 min at RT. 1:2000 anti-mouse IgG coupled to Alexa Fluor A488 secondary antibody (Invitrogen) was added to the nuclei and incubated for 2 h at 4 °C in the dark. Coverslips were rinsed 3 times with 1x PBS for 10 min at RT. Coverslips

were mounted onto glass slides with 3 μL Fluoromount-G mounting medium with DAPI (Invitrogen 00–4959–52). Images were acquired using a Leica SPE confocal microscope. Tau1 and DAPI fluorescence intensity of every nucleus were quantified with Image J software (NIH). Pearson's Chi-squared statistical testing was performed in R (version 1.1.447) to determine significance levels.

2.11. Single-nucleus genome amplification, sequencing and cell-cycle analysis

Nuclei were lysed in RLT plus buffer (Qiagen 1053393) after sorting into individual wells of a FrameStar® 96-well plate. Lysed DNA was diluted in 25 μL wash buffer (50 mM Tris-HCl pH8.3, 75 mM KCl, 3 mM $MgCl_2$, 0.5 % Tween-20, 1 mM DTT) and precipitated using AMPure PCR Clean beads (Beckman Coulter) in an automated liquid handling robotic platform (Hamilton). In more detail, a 1:1 ratio bead to DNA volume was added and incubated for 20 min. The plate was transferred to an LE magnet plate (Alpaqua) for collection of the gDNA for 20 min. Supernatant was removed and gDNA was washed 2 times with 80 % ethanol. Picoplex WGA (Takara) was used for single-cell whole genome amplification according to the manufacturer's instructions at ½ volumes. Amplified gDNA was purified with a 1:1 ratio Ampure beads and eluted in EB buffer to reach a concentration of approximately 10 ng/μL. Dilution of the gDNA to 0.200 ng/μL and subsequent library preparation with Nextera XT DNA Library Preparation kit (Illumina) in 1/10 volumes was executed on an Echo 525 acoustic liquid transfer device (Labcyte). Single-cell gDNA libraries were multiplexed, purified with a 1:0.6 ratio Ampure beads and single end 50 bp read sequenced on a P2 flowcell of the NextSeq 2000 sequencing device (Illumina) aiming at 1 million reads per cell. Genomic read alignment and estimation of genomic copy-number variation was executed according to Macaulay et al. (2015, 2016) with minor modifications. In brief, single-end sequencing reads were demultiplexed and aligned to the GFCh37 human reference genome with BWA-MEM (Li et al., 2013) (Version 0.7.17-r1188). PCR-duplicated reads were removed with Picard (Version 2.21.4) (http://broadinstitute.github.io/picard/). LogR per genomic, nonoverlapping bin of 500,000 uniquely mappable positions was calculated as the read count of that given bin divided by the average read count of the bins genome-wide. %GC correction was performed using a Loess fit in R and LogR values were normalized according to the median LogR genome-wide. Using piecewise constant fitting (PCF) with the penalty parameter, γ, set to 10, the corrected LogR values were segmented into regions with a similar ploidy. Integer DNA copy numbers (CN) were estimated as 2^{logR_*} ψ, with the average ploidy of the cell, ψ, determined as the average CN value with the lowest penalty from a 1.2–6 grid with possible CN values, transformed from segmented LogR values. High penalty values are given to a possible average CN when the sum of squared differences between the unrounded and rounded CN is high.

2.12. Neuroblastoma cell culture

SH-SY5Y cells were cultured in complete medium DMEM (Dulbecco's Modified Eagle's Medium, Invitrogen) with 10 % of fetal bovine serum (Gibco), L-glutamin (2 mM) and penicillin/streptomycin (50 U/ml) in a controlled atmosphere with 5 % of CO_2 at 37 °C. Immunofluorescence on neuroblastoma cells was performed as described previously (Dourlen et al., 2007).

3. Results

3.1. In AD brains, cell cycle markers colocalize with nuclear hypophosphorylated tau in a subpopulation of neurons in the vicinity of amyloid plaques

To explore the link between cell cycle re-activation and different forms of tau in single cells in AD brains, we stained coronal sections of human cortex from AD (Braak VI) and non-demented control (C) patients with Ki67, a general cell cycle marker (Sun et al., 2018) and several phospho-dependent tau antibodies. Hyperphosphorylated tau (hyperP tau) is not uniformly present within the cortex. In particular, neurons exhibiting hyperphosphorylated tau are present in zones next to which are neighboring neurons whose cytoplasm is devoid of phosphorylated tau showing that within the same region very different stages of tau pathology may coexist, reflecting different stages of the disease process. We confirmed a previously found correlation between cytoplasmic and nuclear phosphorylated tau and Ki67 staining in AD brain regions positive for neurofibrillary tangles (NFT)-like hyperP tau (Supplementary Fig. 1a, left panel) (Smith and Lippa, 1995). As expected, in NFT-negative brain regions, this correlation was absent (Fig. 1a). Instead, we observed a correlation between nuclear hypoP tau and Ki67 (Fig. 1a). Interestingly, this population of cells with nuclear colocalization of Ki67 and Tau1 consists exclusively of neurons since all cells are positive for the neuron-specific NeuN marker (Fig. 1b,c). Surprisingly, although neurons with nuclear Tau1 or Ki67 were detected, this Ki67/Tau1 double positive cell population was absent in control brains indicating the AD disease-specific nature of this cellular population (Fig. 1b). Quantification of neuronal Ki67 and Tau1 immunofluorescence (IF) confirmed a significant increase of both nuclear Ki67 and Tau1 in neurons from AD compared to control brains (Fig. 1d). Furthermore, quantification of nuclear Tau1 IF in neurons with or without nuclear Ki67 expression ($Ki67^+$ and $Ki67^-$ respectively) revealed a statistically significant increase of Tau1 in $Ki67^+$ compared to $Ki67^-$ neurons (Fig. 1e) although not all neurons expressing nuclear Ki67 displayed increased nuclear Tau1 labeling (Fig. 1e). Regression analyses showed a statistically significant Pearson correlation coefficient ($r = 0.6607$; $P < 0.0001$) between nuclear Ki67 and Tau1 immunofluorescence intensity in neurons indicating an association between cell cycle activation and nuclear hypoP tau content (Fig. 1f). With a general tau antibody we were able to show that this correlation is not antibody dependent. As for Tau1, total tau nuclear labeling colocalized with Ki67 and NeuN, confirming that tau is indeed present inside the nucleus in a subpopulation of the cycling neurons (Supplementary Fig. 1b). Together, these data thus reveal an AD-specific subpopulation of cycling neurons with a highly hypophosphorylated state of tau in the nucleus (henceforth referred to as $ntau^+$ cycling neurons).

Interestingly, a diffuse DAPI staining was systematically observed in the vicinity of $ntau^+$ cycling neurons (stars show DAPI plaques in the close vicinity of $ntau^+$ cycling neurons in Figs. 1c,2a,4a and Supplementary Fig. 1b,2a,2b). This typical DAPI staining pattern is known to correspond to the presence of chromatin inside the core of amyloid plaques (Pensalfini et al., 2014) (Supplementary Fig. 1c, stars). Using anti-Abeta antibody, we confirmed that $ntau^+$ cycling neurons are present near Abeta plaques (Supplementary Fig. 1d, stars). Furthermore, $ntau^+$ cycling neurons were only found in AD brain with a high load of amyloid plaques (Thal score 5), suggesting that pathological forms of Abeta could play a role in nuclear tau increase and cell cycle reactivation.

$Ntau^+$ cycling neurons represent an average of 58.68 % among all the cycling neurons, within 100 μm around DAPI plaques (Supplementary Fig. 1e).

3.2. Elevated nuclear tau is specifically associated with G1 to S markers in cycling neurons

Although Ki67 is present throughout the cell cycle, its expression level increases from G1 to M phase during the cell cycle (Miller et al., 2018). Therefore, the observed correlation between nuclear tau and Ki67 could indicate that there is a subpopulation of cycling neurons that have passed the G1/S checkpoint. To explore this hypothesis, we used IF to analyze colocalization of hypoP tau with various cell cycle markers specifically expressed during the G1, S, G2 and/or M phases (Fig. 2b).

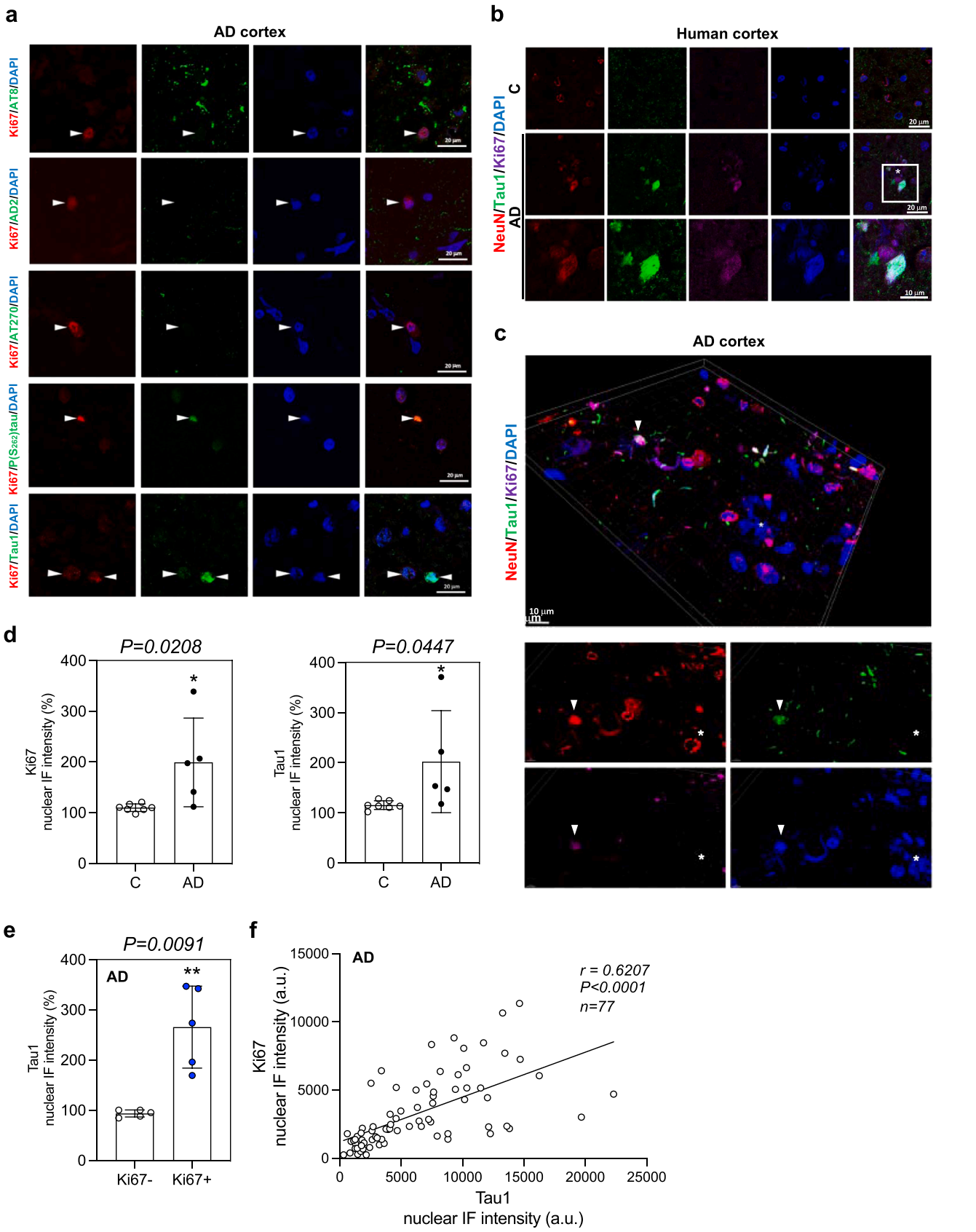

(caption on next page)

Fig. 1. : Hypophosphorylated tau is present in a subpopulation of cycling neuronal nuclei from AD brains. a. Representative images of coronal sections from human post-mortem control (C) and Alzheimer (AD) brain (C: n = 3; AD: n = 5). The sections were labeled with the anti-Ki67 antibody, and with various phospho-dependent anti-tau antibodies. IF signals were analyzed by confocal laser-scanning microscopy (clsm) (z projection). Nuclei were detected with DAPI staining. The scale bars represent 20 μm. Arrowheads show Ki67 positive cells. b. Representative images of coronal sections from control (C) and Alzheimer (AD) brain (C: n = 3; AD: n = 5). The sections were labeled with DAPI and the anti-Ki67, anti-NeuN and Tau1 antibodies. IF signals were analyzed by clsm (z projection). The scale bars represent 20 μm. c. Representative images of the 3D reconstruction of coronal sections from AD brain (n = 5). The sections were labeled with the anti-Ki67, anti-NeuN and Tau1 antibodies. IF signals were analyzed by clsm (z projection). The scale bars represent 10 μm. White arrowhead shows ntau$^+$ cycling neuron. Stars show DAPI plaque. d. The nuclear Ki67 (left panel) and Tau1 (right panel) IF intensity were separately quantified within the same neurons (C: n = 46, AD: n = 68) from C (n = 7) and AD (n = 5) brain. Graphs show the mean of fluorescence per category (Ki67: C= 109,7 %, AD=199.1 %; Tau1: C=115.4 %, AD=202.2 %). 100% corresponds to the mean of non specific fluorescence. Each biological replicate corresponds to one brain. Data are presented as mean ± SEM (*$P < 0.05$; Two-tailed, unpaired Student's t-test). e. The nuclear Tau1 IF intensity was quantified within neurons from AD brain (n = 5) with (Ki67 +)(n = 35) or without (Ki67-)(n = 32) Ki67 signals. Graph shows the mean of fluorescence per category. Each biological replicate corresponds to one brain. Data are presented as mean ± SEM (**$P < 0.01$; Two-tailed, unpaired Student's t-test). f. Graph shows the correlation between the intensity of the nuclear Ki67 and Tau1 IF signals within the same neurons (n = 77) from AD brain (n = 5). Pearson coefficient: r = 0,6207 ($P < 0.0001$).

We found that the nuclear accumulation of hypoP tau starts early in the G1 phase as shown with the cyclin D1 marker, and persists in late G1 and S phase, illustrated by PCNA and cyclin A markers (Fig. 2a,c). A weak nuclear Tau1 labeling can be observed in cyclin B1-expressing neurons reflecting the ability of these neurons to fully replicate their DNA and enter G2 (Fig. 2a). Quantification did not show a statistically significant increase in hypoP tau in cyclin B1-positive neurons compared to non-cycling neurons (Fig. 2c) suggesting that the majority of ntau$^+$ cycling neurons do not reach the G2 phase. However, these data don't exclude that some of these neurons become tetraploid and enter G2. The absence of PH3 indicates that these neurons do not reach M-phase which is in accordance with full but also partial replication of the genome (Supplementary Fig. 2a).

3.3. Ntau$^+$ neurons with increased DNA content exclusively arise in AD brains

Since nuclear tau appears to accumulate during S phase, we investigated whether ntau$^+$ cycling neurons regain the capacity to replicate DNA. We quantified the DAPI fluorescent signal (López-Sánchez et al., 2017) in ntau$^+$ cycling neurons and compared it with non-cycling neurons in AD brains to determine whether the DNA content in this ntau$^+$ subpopulation of neurons was altered. Indeed, a significantly increase of DAPI fluorescence intensity in the ntau$^+$ cycling neurons compared to non-cycling neurons was detected (Fig. 3a). Subsequently, we speculate that this altered DNA content is due to a, at least partial, replication of the DNA. Hence, the relationship between nuclear tau, increased DNA content and neuronal cell cycle in AD brains was further explored by means of FANS analysis (Supplementary Fig. 3) followed by IF and single-nucleus genome sequencing of isolated nuclei (Fig. 3b-f). In FANS, the mean DAPI area (DAPI-A) intensity signal is considered to represent a population of neurons with a normal diploid genome (2 C/2 n), while a DAPI-A value of this mean DAPI-A multiplied by two represents a fully replicated genome (4 C/4 n) (Fig. 3b). We consider the DNA content of a neuron increased when the DAPI-A intensity signal exceeds the threshold of the mean DAPI-A signal in the sample plus two standard deviations. As demonstrated by FANS analysis of post-mortem human donor brains, a significantly higher percentage of neurons with increased DNA content (>2 n neurons) could be detected in AD compared to control brains ($P < 0.01$) (Fig. 3b,c). More specifically, in AD brains, 2.84 % (1.9–10.7 %) of the neurons have an increased DNA content, while control brains contain 1.69 % (1.2–2.3 %) of neurons with increased DNA content (Fig. 3c). Surprisingly, the DAPI-A values for the majority of neurons do not reach the 4n-representative value, which indicates most neurons have not yet fully replicated their genomes. Remarkably, one donor brain with a low amyloid beta load (Thal 1), which was classified as an atypical AD case, merely contained 1.7 % of neurons with increased DNA content (Fig. 3c), strengthening the finding that cycling neurons with increased DNA content are found more frequently in AD brains associated with high amyloid plaques loads (Fig. 1, Supplementary Fig. 1).

For illustrative purposes only, a limited number of neuronal nuclei with increased DNA content were sorted and subjected to single-nucleus genome sequencing. An oscillating pattern of the estimated integer DNA copy number ($2^{\log} * \boldsymbol{\psi}$ with $\boldsymbol{\psi}$ = average ploidy) was observed, which is reported to be characteristic for DNA replication and typically observed in cells in S-phase (Van der Aa et al., 2013) (Fig. 3d,e, Supplementary Fig. 3f,g,h). Taken together with the FANS analysis, where the majority of neurons with an increased DNA content demonstrate an incomplete replication of their genome (Fig. 3b), this indicates that these neurons most likely find themselves blocked in S-phase. Nevertheless, since our single-cell genome sequencing analysis pipeline cannot differentiate between a diploid and a tetraploid copy number profile, we do not exclude the possibility that at least part of the neurons with increased DNA content have fully replicated their genome. Importantly, these neurons with increased DNA content can be found in both AD and control brains, however, the abundance is higher in AD brains (Fig. 3b, c).

An exclusive presence of nuclear tau (Tau1$^+$) in AD pathology neuronal nuclei was demonstrated through Tau1 IF staining of single nuclei, isolated from AD and control brains (Fig. 3f). It can be noted that, unlike the diffuse nuclear labeling of Tau1 in ntau$^+$ cycling neurons revealed by IF in AD brain sections (Figs. 1,2), Tau1 labeling in isolated neurons analyzed by FANS is mainly localized within the nucleus close to the inner nuclear membrane. This difference in detection is probably due to technical constraints related to the multiplicity of steps in the FANS analysis. Interestingly, the localization of tau in the nuclear periphery directly below the nuclear membrane corresponds to the predominant presence of pericentromeric heterochromatin where tau binding has been described (Mansuroglu et al., 2016). No tau expression (Tau1$^+$) could be detected in neuronal nuclei with increased DNA content (>2 n) selected and sorted from control brains in contrast to these isolated from AD brains. A significant number of neuronal nuclei with increased DNA content derived from AD brains were positive for tau (Tau1$^+$) ($P < 0.0001$) (Fig. 3g, left panel). Interestingly, tau could also be detected in the nuclei of diploid neurons (2 n) selected and sorted from AD brains (Fig. 3g, right panel), but was significantly increased in neuronal AD nuclei with an increased DNA content ($P < 0.001$) (Fig. 3 g, right panel).

Altogether these results validate the accumulation of nuclear tau in a subpopulation of neurons with increased DNA content, exclusively from AD brains, and suggest that those neurons which have passed the G1/S checkpoint mainly remain blocked in S phase.

3.4. Increased DNA damage, elevated nuclear tau, and cell cycle reactivation are simultaneously induced under oxidative stress in neurons

Because oxidative stress is linked to cell cycle reactivation (Klein et al., 2003; Kagias et al., 2012), increased nuclear tau expression (Sultan et al., 2011; Violet et al., 2014) and Abeta plaques (Swomley et al., 2014), which are found in the vicinity of ntau$^+$ cycling neurons (see above), we explored oxidative stress as a potential mechanism

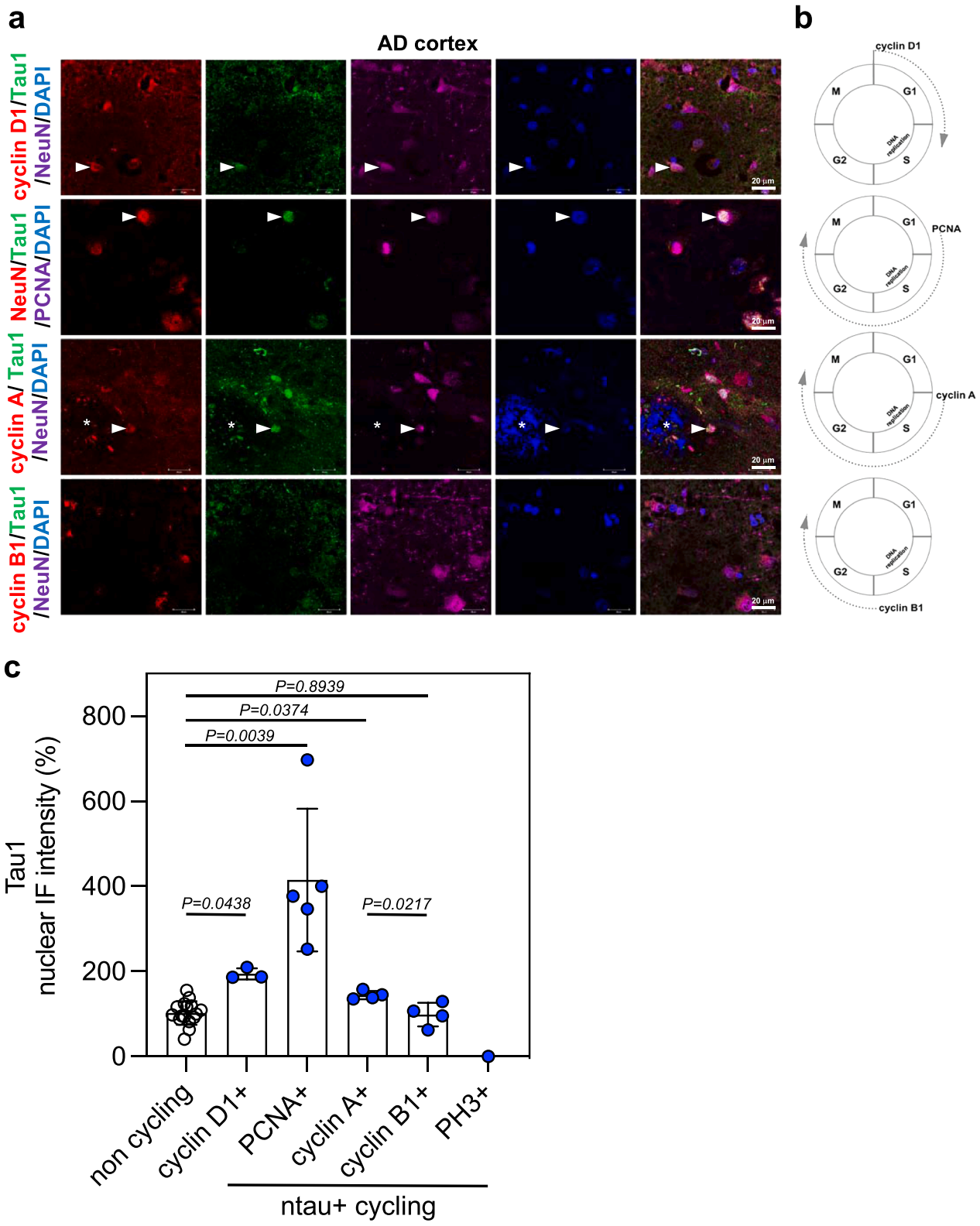

Fig. 2. : Nuclear tau is present in cycling neurons during G1 and S phases. a. Representative images of coronal sections from human post-mortem AD brain (n = 3–5). The sections were labeled with antibodies against cell cycle proteins specifically expressed during different phases (cyclin D1; PCNA; cyclin A; cyclin B1), NeuN and Tau1. Immunofluorescence signals were analyzed by clsm (z projection). Nuclei were detected with DAPI staining. The scale bars represent 20 µm. Arrowheads show Tau1 positive neurons. Stars show DAPI plaque. b. Schematic representation of the expression of cell cycle proteins cyclin D1, PCNA, cyclin A and cyclin B1 during the cell cycle. c. The intensity of the nuclear Tau1 IF signals was quantified within non-cycling (n = 54) or cycling neurons from human post-mortem AD brain (n = 3–5) expressing the cell cycle marker cyclin D1 (n = 31), PCNA (n = 52), cyclin A (n = 34), cyclin B1 (n = 20) or PH3. Graph shows the mean of fluorescence per category. Each biological replicate corresponds to one brain. Data are presented as mean ± SEM (**$P < 0.01$; *$P < 0.05$; Two-tailed, unpaired Student's t-test).

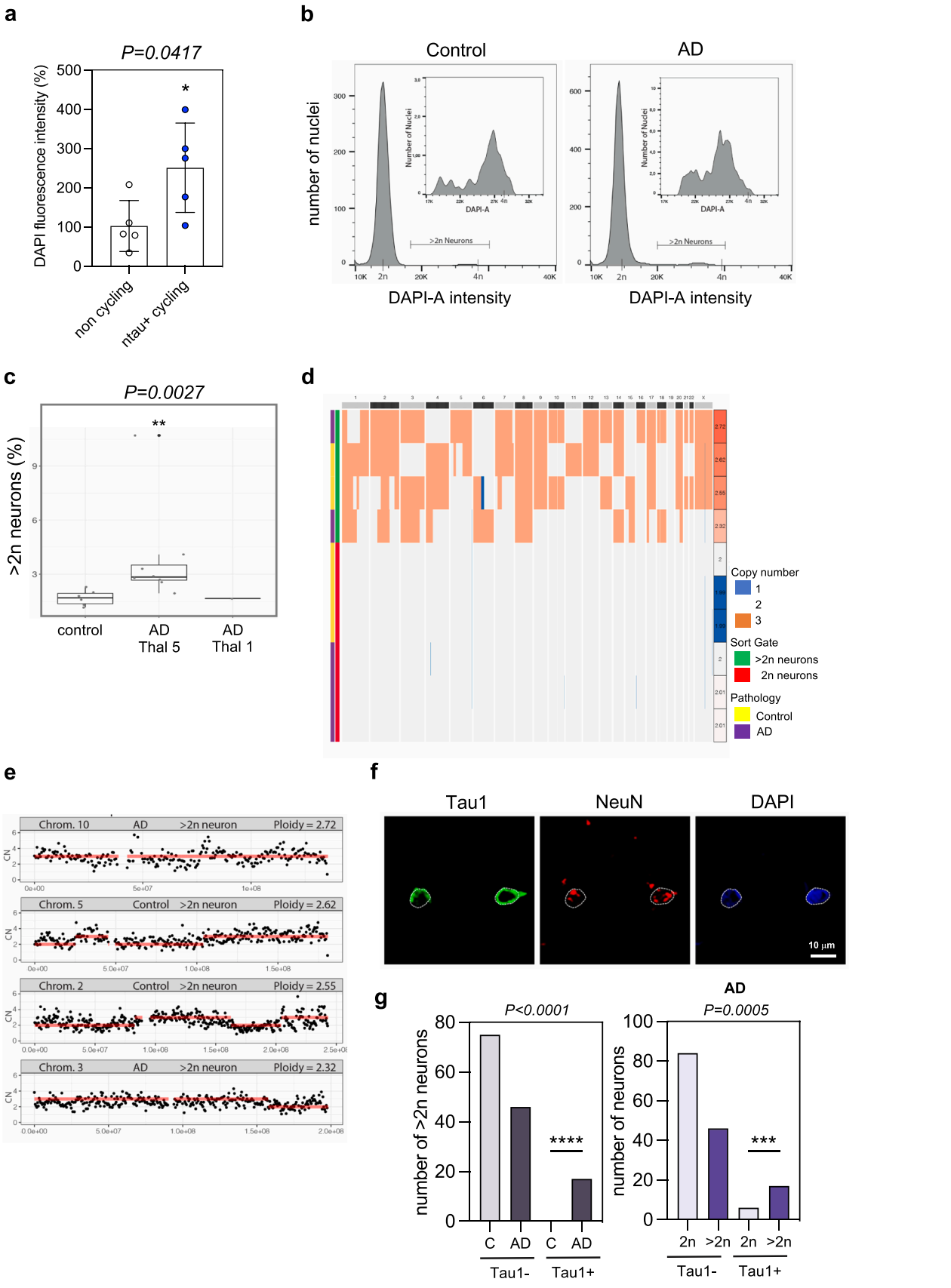

(caption on next page)

Fig. 3. : FACS, single nucleus genome sequencing and immunofluorescent analysis of neuronal nuclei with increased DNA content. a. DAPI fluorescence intensity was quantified within non-cycling (n = 44) and ntau$^+$ cycling (n = 70) neurons from AD brain (n = 5). Graph shows the mean of nuclear fluorescence per category. Each biological replicate corresponds to one brain. Data are presented as mean ± SEM (*$P < 0.05$; Two-tailed, unpaired Student's t-test). b. Linearly scaled, DAPI pulse area (DAPI-A) intensity signals of neuronal nuclei from a control and AD brain. The DAPI-A signal cutoffs for DNA content exceeding a diploid genome signal (>2 n) and 2 n and 4 n DAPI-A intensities are indicated. Set-ins represent enlargements of the DAPI-A intensity signal of > 2 n neurons. c. Boxplots representing the percentage of > 2 n neuronal nuclei from control brain (n = 5), AD brain (Thal score 5) (n = 8) and AD brain (Thal score 1) (n = 1) (**$P < 0.01$; Unpaired two-samples Wilcoxon test). Each biological replicate corresponds to one brain. d. Heatmap of four > 2 n neuronal nuclei (red) and six 2 n neuronal nuclei (green) derived from AD (purple) and Control (yellow) brain. X-axis depicts chromosomes. Average ploidy (ψ) per nucleus is shown in the rightmost column of the heatmap. Copy number is indicated in red when gained and blue when deleted. e. Illustrative examples of representative copy number profiles of one chromosome for each > 2 n neuron. X-axis depicts position on the chromosome. Y-axis represents ploidy. Black dots represent ploidy of individual 500 kb bins. Red line indicates estimated ploidy per segment. f. Representative confocal images of > 2 n neuronal nuclei from AD brain (n = 5) sorted on coverslips and stained with DAPI and anti-NeuN and Tau1 antibodies. Nuclei are delimitated by white dashed lines. The scale bar represents 10 μm. g. Left Bar plot represents the absolute number of > 2 n neuronal nuclei selected and sorted from C (light gray, n = 63) versus AD (dark gray, n = 75) brain (C: n = 5; AD: n = 5) with (Tau1 +) or without (Tau1) expression of ntau, (**** $P < 0.0001$; Unpaired two-samples Wilcoxon test). Each biological replicate corresponds to one neuron. Right bar plot represents the absolute number of 2 n (light blue, n = 90) and > 2 n neurons (dark blue, n = 63) with (Tau1 +) or without (Tau1-) ntau expression, selected and sorted from AD brains (n = 5) (***$P < 0.001$; Pearson's Chi-squared test). Each biological replicate corresponds to one neuron.

linking these phenomena. Hence, we investigated whether oxidative stress-induced DNA damage could be an underlying cause of the simultaneous neuronal cell cycle re-activation and nuclear tau accumulation in AD brains. We analyzed by IF the presence of 8-oxo-7, 8-dihydroguanine (8-oxo-G), the earliest and most frequent oxidative DNA lesion in neurons from control and AD brain (Fig. 4a). Strikingly, ntau$^+$ cycling neurons from AD brains were burdened with oxidative DNA damage (Fig. 4b). A significant positive correlation between 8oxoG and Tau1 IF intensity was observed in ntau$^+$ cycling neurons ($r = 0.5582$; $P < 0.0001$) (Fig. 4c), confirming an association between the level of oxidative DNA damage and nuclear tau content. Similar results were obtained using PCNA as an additional indicator of proliferation instead of Ki67 (Supplementary Fig. 4a-c).

Since DNA double strand breaks (DSB) can be an indirect consequence of oxidative stress, we evaluated the presence of a phosphorylated form of Histone H2AX (PSer139-H2AX; H2AX), a marker for initiation of DSB repair. In neurons from control and AD brains (Supplementary Fig. 5a), γH2AX labeling was mainly observed in cells from AD brains. The level of γH2AX was slightly, although significantly higher in ntau$^+$ cycling compared to non-cycling neurons from AD brains (Supplementary Fig. 5b). However, regression analysis between γH2AX and Tau1 IF intensity ($r = 0.1813$; $P = 0.2076$) (Supplementary Fig. 5c) in ntau$^+$ cycling neurons failed to show any significant correlation ($r = 0.1813$; $P = 0.2076$) (Supplementary Fig. 5c). Taken together, these results suggested that oxidative DNA damage can trigger cell cycle re-entry with nuclear accumulation of tau in neurons while DSB do not appear to be involved.

To further substantiate this finding, differentiated cultured neurons were subjected to an acute but subtoxic oxidative stress or PBS treatment (Sultan et al., 2011). The effects of those treatments on the levels of nuclear oxidative DNA damage, DSB, tau and the cell cycle markers Ki67 and PCNA were analyzed as described above for AD brains. Administration of a subtoxic concentration of hydrogen peroxide (H_2O_2) to neurons is already known to induce oxidative DNA damage, DSB, cell cycle re-entry (Schwartz et al., 2007) and even nuclear tau accumulation (Sultan et al., 2011). Indeed, H_2O_2 treatment in neuronal cultures strongly increased the nuclear level of Tau1, Ki67, PCNA, 8-oxo-G (Fig. 4d,e,f,h) (Supplementary Fig. 4d,e) and γH2AX (Supplementary Fig. 5d,e) in neurons demonstrating that oxidative stress can simultaneously trigger DNA damage, nuclear accumulation of tau and cell cycle reactivation in differentiated neurons. Moreover, a similar correlation, as in post-mortem AD brain sections (Fig. 1f), was observed between Ki67 and Tau1 immunofluorescence ($r = 0.5500$; $P < 0.0001$) (Fig. 4g) in culture. In addition, the other correlations found in the AD brains were replicated in cultured neurons. Nuclear tau correlates with oxidative DNA damage ($r = 0{,}5848$; $P = 0{,}0011$) (Fig. 4i) and ($r = 0{,}8008$; $P < 0{,}0001$) (Supplementary Fig. 4f) but not with the formation of DSB ($r = 0.1919$; $P = 0.1224$) (Supplementary Fig. 5f) in neuronal cultures, as previously observed in post-mortem AD brains.

To test whether joint nuclear tau increase and cell cycle re-entry in differentiated cultured neurons was restricted to an acute oxidative stress, we tested the effect of *tert*-Butyl hydrogen peroxide (tBut-H_2O_2), a more stable but less reactive H_2O_2 analog, at identical concentration (1 mM) and time (1 H) as H_2O_2 (Supplementary Fig. 6a). Supplementary Fig. 6 shows that although treatment with tBut-H_2O_2 causes around 10 times less oxidative damage (8-oxo-G) (Supplementary Fig. 6b) than H_2O_2 (Fig. 4h), it induces similar effects but in lesser amplitudes on nuclear levels of Tau1 (Supplementary Fig. 6c) (Fig. 4e) and Ki67 (Supplementary Fig. 6d) (Fig. 4f), indicating that nuclear tau accumulation and cell cycle reactivation in neurons can be induced as well under milder oxidative stress.

Both in AD brains and primary neuronal cultures, a clear link between oxidative DNA damage, cell cycle reactivation and nuclear tau levels in neurons can be observed, which strongly suggest that, early in AD pathogenesis, neurons facing oxidative stress-induced DNA damage undergo nuclear tau accumulation as well as cell cycle re-activation as part of an emergency DNA damage response.

Beside, H_2O_2 treatment caused BrdU incorporation correlated to nuclear tau augmentation and cyclin A expression indicating DNA replication occurs in ntau$^+$ neurons under oxidative stress (Supplementary Fig. 7a-e).

Importantly, similar to our observations in ntau$^+$ cycling neurons from AD brains (Supplementary Fig. 2b), we did not detect cleaved caspase 3 (the activated form of the apoptosis-associated enzyme) or chromatin fragmentation in cultured ntau$^+$ cycling neurons under oxidative stress condition (Supplementary Fig. 5g) reflecting an absence of apoptotic mechanisms. On the contrary, cleaved caspase 3 was clearly present in cells lacking nuclear tau, suggesting that the presence of nuclear tau might be neuroprotective.

3.5. *Downregulation of tau prevents neuronal cell cycle progression into S phase triggered by oxidative stress*

Our results indicated that oxidative stress can co-induce neuronal cell cycle re-entry and nuclear tau accumulation in response to elevated oxidative DNA damage. To investigate whether these two events act independently of each other or whether there is a relationship between the two, we analyzed the role of tau downregulation on the expression of various proliferation markers and on the DNA level of cycling neurons, in differentiated neuronal cultures. Neuronal cultures from wild type mouse brain embryos (7 DIV) were infected or not with a lentiviral vector (LV) encoding short hairpin (sh) RNA targeting tau and expressing the GFP reporter gene (LV-shtau) or shRNA control (LV-shctrl) targeting GFP which is not endogenously expressed in neurons (Supplementary Fig. 8a). Infection with LV-shtau strongly decreased tau expression by an average of 75 % as revealed by WB (Supplementary Fig. 8b) and with an average of 70 % in neuronal nuclei analyzed by IF (Fig. 5a) while shctrl had no significant effect (Fig. 5a; Supplementary

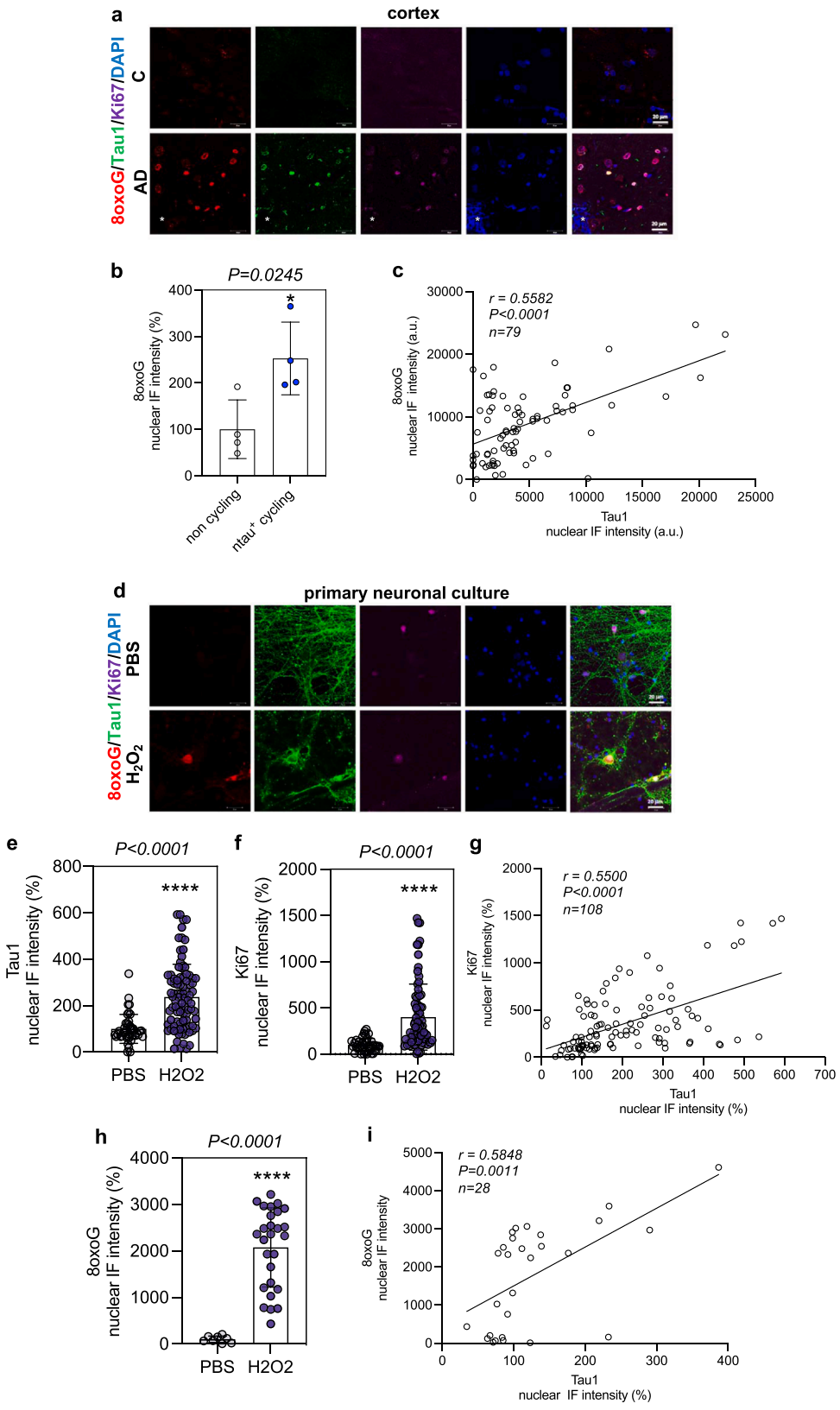

Fig. 4. : Oxidative stress induces joint DNA damage, nuclear tau increase and cell cycle reactivation in neurons. a. Representative images of coronal sections from C (n = 4) and AD (n = 4) brain. The sections were labeled with the anti-8oxoG, anti-Ki67 and Tau1 antibodies. IF signals were analyzed by clsm (z projection). Nuclei were detected with DAPI staining. The scale bars represent 20 μm. Stars show DAPI plaque. b. The intensity of the 8oxoG and Tau1 IF signals were separately quantified within the same non-cycling (n = 48) and ntau^{+} cycling (n = 99) neurons from AD brains (n = 4). Graph shows the mean of nuclear 8oxoG fluorescence per category. Each biological replicate corresponds to one brain. Data are presented as mean ± SEM (* $P < 0.05$; Two-tailed, unpaired Student's t-test). c. Graph shows the correlation between the intensity of the nuclear 8oxoG and Tau1 IF signals in the same neurons (n = 79). Pearson coefficient: r = 0,5582 ($P < 0.0001$). d. Representative images of primary neuronal cultures treated one hour with H_2O_2 (1 mM) or PBS. Coverslips were labeled with DAPI and the anti-8oxoG, anti-Ki67 and Tau1 antibodies. Immunofluorescence signals were analyzed by clsm (z projection). Scale bars represent 20 μm. The intensity of the nuclear Tau1 e. and Ki67 f. fluorescence signals were separately quantified within the same neurons (PBS: n = 42, H_2O_2: n = 91) from five different cultures. Graphs show the mean of nuclear fluorescence per category. Each biological replicate corresponds to one cell. Data are presented as mean ± SEM (****$P < 0.0001$; Mann Whitney U test). g. Graph shows the correlation between the intensity of the nuclear Ki67 and Tau1 IF signals in the same neurons (n = 108) after H_2O_2 treatment. Pearson coefficient: r = 0,5500 ($P < 0.0001$). h. The intensity of the nuclear 8oxoG IF signals was separately quantified in parallel to Tau1 in two different cultures (PBS: n = 8, H_2O_2: n = 27). Graphs show the mean of nuclear fluorescence per category. Each biological replicate corresponds to one cell. Data are presented as mean ± SEM (**** $P < 0.0001$; Mann Whitney U test). i. Graph shows the correlation between the intensity of the nuclear 8oxoG and Tau1 fluorescence signals in the same neurons (n = 28) after H_2O_2 treatment. Pearson coefficient: r = 0,5848 ($P = 0.0011$).

Fig. 8b). Infected neuronal cultures (24 DIV) were subjected to H_2O_2 or PBS treatment as previously described (Fig. 4d). Along with increasing nuclear tau, H_2O_2 treatment increased the nuclear level of the G1 marker cyclin D1, the G1/S marker PCNA, the S marker cyclin A and the DNA level as measured by DAPI fluorescence, compared to PBS treatment, in ntau^{+} cycling neurons (Supplementary Fig. 9a,b,d,e; Fig. 5b,c,e). These results indicated that the oxidative stress condition can induce cell cycle progression to S phase and at least initiate DNA replication in differentiated neurons.

The effect of tau downregulation was analyzed on the expression of

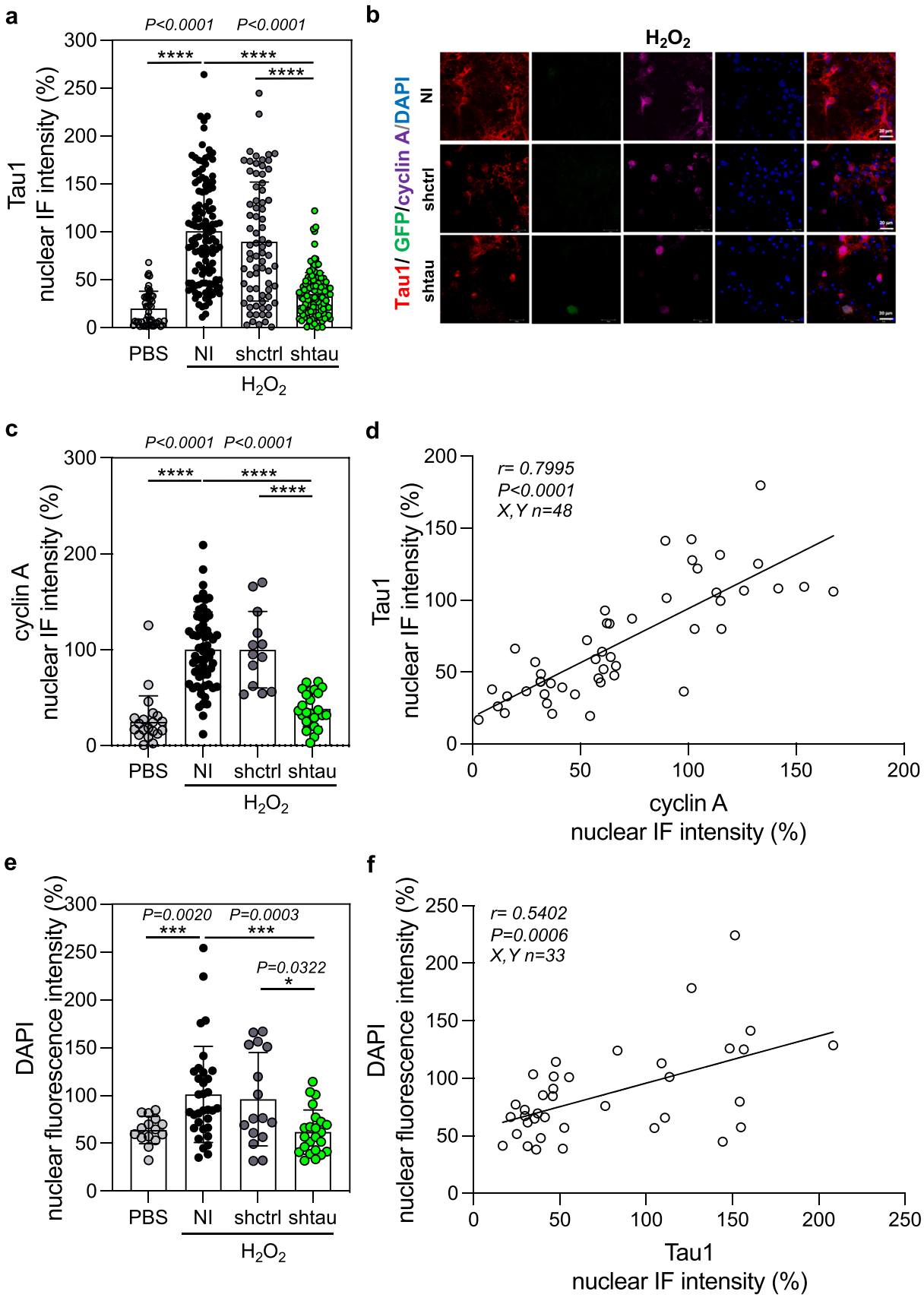

(caption on next page)

Fig. 5. : Tau downregulation prevents the cyclin A and DNA content increase in neurons under oxidative stress. a. Quantification of the intensity of Tau1 IF signals in primary neuronal cultures (n = 5) untreated (PBS: n = 46) or treated with H_2O_2 (1 mM, 1 H) and non-infected (NI: n = 119) or infected with the LV-shctrl (shctrl: n = 74) or the LV-shtau (shtau: =116). Graph shows the mean of nuclear Tau1 fluorescence per category. Each biological replicate corresponds to one cell. Data are presented as mean ± SEM (****$P < 0.0001$; Mann Whitney U test). b. Representative images of primary neuronal cultures treated with H_2O_2 and non-infected (NI: n = 63) or infected with the LV-shctrl (shctrl: n = 13) or the LV-shtau (shtau: n = 24). Coverslips were labeled with DAPI and the anti-cyclin A and Tau1 antibodies. Immunofluorescence signals were analyzed by clsm (z projection). The scale bars represent 20 μm. c. The intensity of the nuclear cyclin A IF signal was separately quantified in parallel to Tau1 within the same neurons from two different cultures (PBS: n = 22; H_2O_2: NI (n = 63), shctrl (n = 13), shtau (n = 24$_)$). Graph show the mean of nuclear IF per category. Each biological replicate corresponds to one cell. Data are presented as mean ± SEM (****$P < 0.0001$; Mann Whitney U test). d. Graph shows the correlation between the intensity of the nuclear cyclin A and Tau1 IF signals in the same neurons (n = 48) after H_2O_2 treatment. Pearson coefficient: r = 0,7995 ($P < 0.0001$). e. The intensity of the nuclear DAPI fluorescence signals was separately quantified in parallel to Tau1 within the same neurons from two different cultures (PBS: n = 15; H_2O_2: NI (n = 33), shctrl (n = 16), shtau (n = 23)). Graph show the mean of nuclear fluorescence per category. Each biological replicate corresponds to one cell. Data are presented as mean ± SEM (*** $P < 0.001$; * $P < 0.05$; Mann Whitney U test). f. Graph shows the correlation between the intensity of the nuclear Tau1 and DAPI fluorescence signals in the same neurons (n = 33) after H_2O_2 treatment. Pearson coefficient: r = 0540$_2$ ($P < 0.0001$).

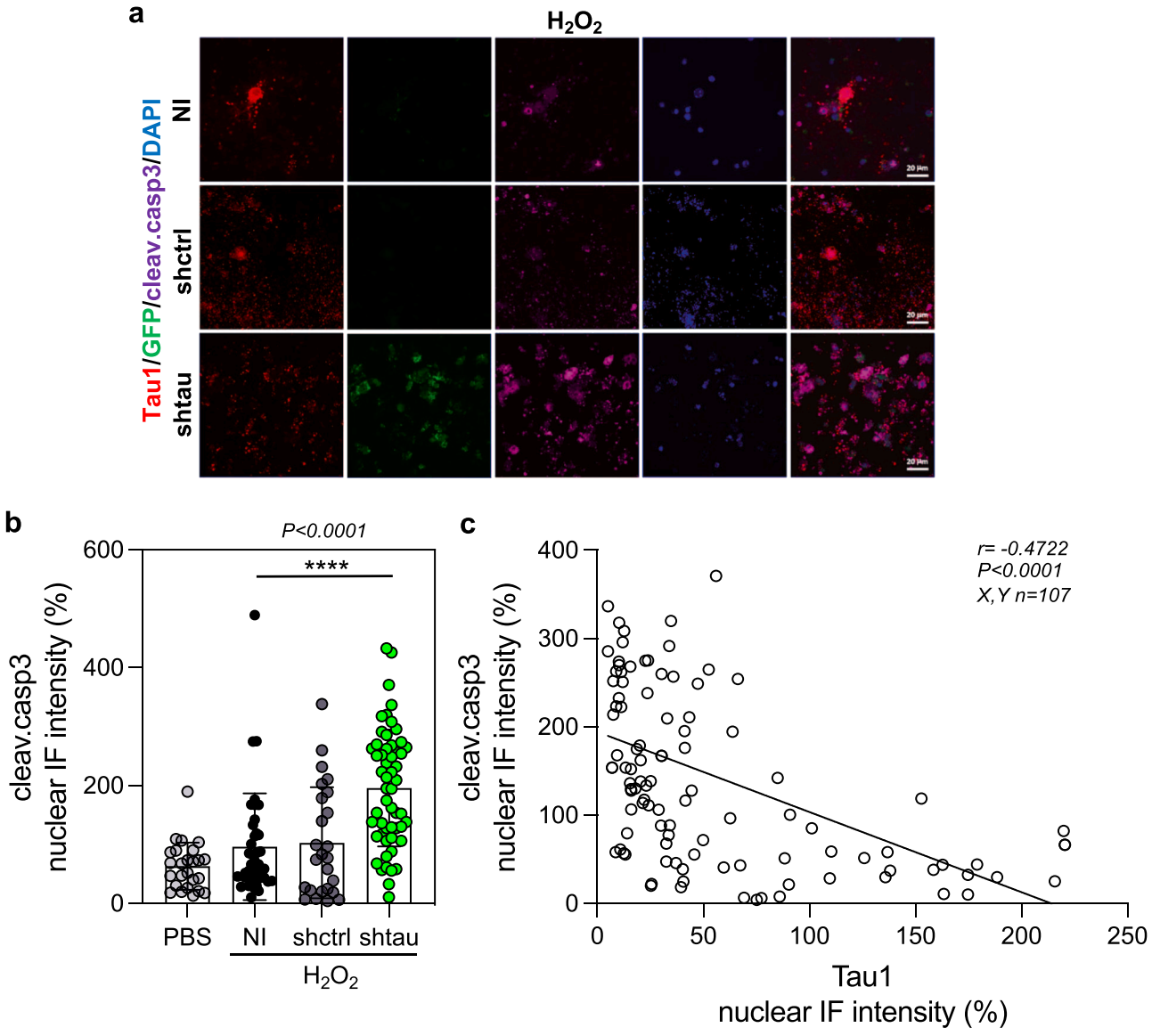

Fig. 6. : Tau downregulation prevents apoptosis activation in neurons under oxidative stress. a. Representative images of primary neuronal cultures treated with H_2O_2. (1 mM, 1 H) and non-infected (NI: n = 39) or infected with the LV-shctrl (shctrl: n = 25) or the LV-shtau (shtau: n = 55). Coverslips were labeled with DAPI and the anti-cleaved caspase 3 and Tau1 antibodies. Immunofluorescence signals were analyzed by clsm (z projection). The scale bars represent 20 μm. b. The intensity of the nuclear cleaved caspase 3 IF signal was separately quantified in parallel to Tau1 within the same neurons from two different cultures (H_2O_2: NI (n = 33), shctrl (n = 16), shtau (n = 23)). Graph shows the mean of nuclear IF per category. Each biological replicate corresponds to one cell. Data are presented as mean ± SEM (****$P < 0.0001$; Mann Whitney U test). c. Graph shows the correlation between the intensity of the nuclear cleaved caspase 3 and Tau1 fluorescence signals in the same neurons (n = 107) after H_2O_2 treatment. Pearson coefficient: r = -0,4722 ($P < 0.0001$).

cyclin D1 (Supplementary Fig. 9a,b), PCNA (Supplementary Fig. 9d,e) and cyclin A (Fig. 5b,c) under H_2O_2 treatment. For each cell cycle marker analyzed, nuclear Tau1 level was quantified in the same neurons.

After H_2O_2 treatment, nuclear tau reduction induced by shtau had no significant effect on the expression of cyclin D1 (Supplementary Fig. 9a, b) and PCNA (Supplementary Fig. 9d,e). No significant association between Tau1 and cyclin D1 (Supplementary Figure 9c), and between Tau1 and PCNA IF was observed (Supplementary Fig. 9f). However, reduction of nuclear tau specifically decreased cyclin A expression (average values: NI=100 %; shtau=36 %) and decreased DNA content (average values: NI=100 %; shtau=61 %) (Fig. 5c,e). Nuclear cyclin A and tau levels were strongly correlated ($r = 0.7995$, $P < 0.0001$) (Fig. 5d). Significant correlation was also observed between nuclear tau and DNA levels ($r = 0.5402$, $P = 0.0006$) (Fig. 5f). Shctrl infection had no effect on the expression of the different markers under H_2O_2 treatment (Fig. 5a,b,c,e; Supplementary Fig. 9a,b,d,e). Similar results on Tau1 and cyclin A were obtained after neuronal infection with LV-shctrl and a lentiviral vector identical to LV-shctrl but which additionally expresses the tomato reporter gene (LV-tomato-shctrl) to view infected neurons (Supplementary Fig. 8e,g,h). The average percentage of neuronal infection was similar after infection with LV-shtau (60 %) and LV-tomato-shctrl (66 %) (Supplementary Fig. 8d,f).

Altogether these results indicate that tau has no effect on the oxidative stress-induced re-entry of neurons in G1 but specifically controls the neuronal cell cycle progression into S phase.

3.6. Downregulation of tau activates apoptosis

An observed increase of cleaved caspase 3 in the absence of nuclear tau in neurons treated by H_2O_2 (Supplementary Fig. 5g), suggested that the presence of tau in the nucleus of ntau$^+$ neurons promotes cell survival under oxidative stress. Hence, we analyzed the effect of tau downregulation on the expression of nuclear cleaved caspase 3 (Kamada et al., 2005) in cultured neurons under oxidative stress (Fig. 6a). The decrease of tau expression was associated with an increase of the level of nuclear cleaved caspase 3 in neurons treated with H_2O_2 (average values: NI=100 %; shtau=196 %) (Fig. 6b). Furthermore, nuclear tau and cleaved caspase 3 levels were inversely correlated ($r = -0.4722$, $P < 0.0001$) (Fig. 6c), demonstrating the protective role for tau to prevent oxidative stress-associated cell death in cycling neurons.

In addition, since neurons with a high rate of DNA damage are preferentially susceptible to cell death after re-activation of the cell cycle, we analyzed whether the activation of apoptosis, induced by the downregulation of tau, could be related to increased oxidative DNA damage. However, decreasing the tau level did not alter the level of 8oxoG, indicating that the level of oxidized DNA in cycling neurons is unrelated to the level of tau (Supplementary Fig. 10a,b). Furthermore, it indicates that neuronal apoptosis, associated to the decrease of tau expression, is not induced by an increase in oxidative DNA damage.

4. Discussion

Here we report the link between hypoP nuclear tau and the cell cycle reactivation in a subpopulation of neurons (ntau$^+$ cycling neurons) from AD brains. Our results highlight an essential role for tau to promote the neuronal cell cycle progression to S phase in response to oxidative DNA damage and maintain cell survival (Fig. 7).

This study demonstrates that in response to elevated oxidative DNA damage, tau is required to permit cycling neurons to progress to S phase. Counterintuitively, although reactivation of the cell cycle is widely considered deleterious, the need for neurons to cross the G1/S checkpoint has been reported to promote neuronal survival (Wartiovaara et al., 2002; Ippati et al., 2021; Nandakumar et al., 2021). In line with these reports, our results reveal a connection between the progression through the S phase and the prevention of neuronal apoptosis in cycling neurons and show that these two events are tau dependent. Recently, Ippati et al. reported that the re-entry of neurons into early S-phase was protective against cellular toxicity induced by oligomeric forms of Abeta (Ippati et al., 2021). Moreover, it has previously been described that cell cycle progression depends on tau in cultured neurons treated by oligomers of the Abeta peptide (Seward et al., 2013). Strikingly, we observed the recurrent presence of ntau$^+$ cycling neurons near amyloid plaques in AD brains with a high Thal score, suggesting a tight relationship between pathological forms of Abeta and the involvement of nuclear hypoP tau in the process of neuronal cell cycle progression and survival. It is therefore tempting to speculate that oxidative stress-induced DNA damage induced by oligomeric forms of Abeta, located into Abeta plaques, may drive tau-dependent S phase progression and promote neuronal survival in AD brains. Conversely we cannot rule out that the presence of plaques close to the S-phase-arrested cells might be a downstream or unrelated event. This potential new interplay between Abeta and tau warrants further investigation.

DNA content evaluation with FANS and IF of single nuclei

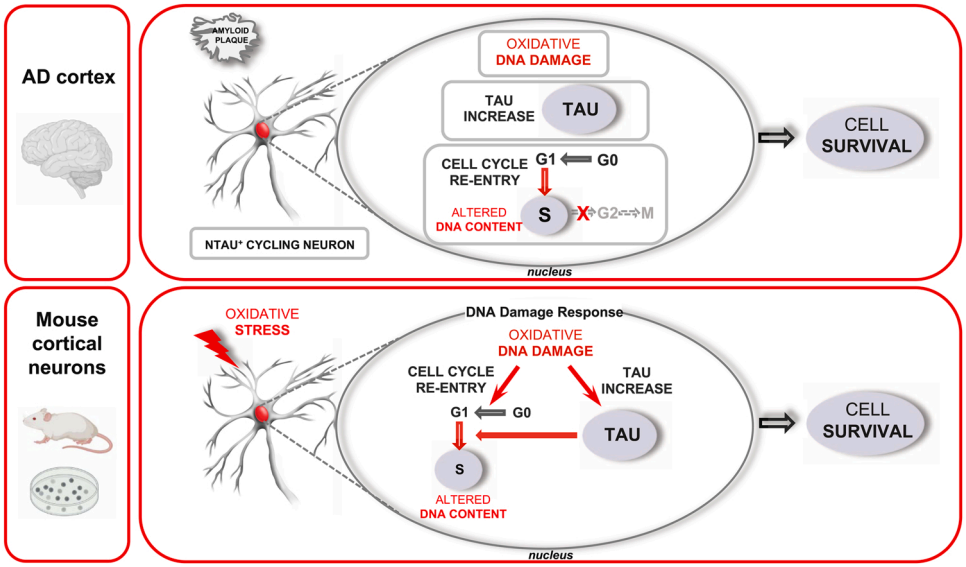

Fig. 7. Schematic summary of the results in AD brains and primary neuronal cultures.

demonstrated the presence of DNA content variation in ntau$^+$ neurons, exclusively derived from AD brains. Additionally, single-cell copy number profiles of neurons with increased DNA content are indicative of altered or incomplete DNA replication, meaning these ntau$^+$ cycling neurons most likely survive while being confined in S phase with a DNA content above the diploid level. Nevertheless, we do not rule out the possibility that a very small part of the neurons in our dataset which are confined in S-phase have nearly or even completely replicated their genome, given that our single-cell whole-genome sequencing analysis pipeline does not allow for differentiation between a single-cell copy number profile of a diploid or a tetraploid neuron. However, while our conclusions are in line with (Westra et al., 2009), who were unable to detect increased levels of tetraploid neurons in AD brains, further experiments with a higher sample size are needed to confirm this conclusion.

Interestingly, an increase in DNA content and polyploidy are employed by various cell types as an adaptive process to tolerate high levels of DNA damage (Nandakumar et al., 2021).

In addition, it is important to stress that the altered amount of DNA in ntau$^+$ cycling neurons contributes to the genomic mosaicism observed at early stages of AD (Fischer et al., 2012; Bushman et al., 2015; Shepherd et al., 2018; Rohrback et al., 2018; Costantino et al., 2021).

Taken together, our results highlight a key role for tau in cell cycle progression and DNA content increase, which likely promotes the survival of neurons in response to an excess of oxidative DNA damage. Therefore, in AD brains, the progression of the neuronal cell cycle to S phase could reflect a tau-dependent protective mechanism employed by neurons in response to high loads of oxidative DNA damage, to prevent cell death, rather than a faux-pas.

In addition, as oxidative stress and reactivation of the neuronal cell cycle are common hallmarks in many neurological disorders (Parkinson Disease, Huntington Disease, Amyotrophic Lateral Sclerosis, ischemia, vascular dementia) (Joseph et al., 2020) it would be worth studying whether tau could play a similar critical role in the cell cycle progress and neuronal survival in these diseases.

We cannot exclude that the prolonged confinement of neurons into S phase, while retaining DNA content variation, could trigger long-term cellular dysfunctions such as increased ferroptotic pressure (Maher et al., 2020; Ma et al., 2022) eventually leading to neuronal vulnerability and delayed neuronal death. However, a potential long term vulnerability of ntau$^+$ cycling neurons would be consistent with their absence in late stages of AD pathology in sub-regions of the cortex from AD brains where neurons exhibit severe tau pathology (i.e., cytoplasmic hyperphosphorylation and NFT). Interestingly, the absence of ntau$^+$ cycling neurons at late stages of the pathology is reminiscent of what has been described by Thomas Arendt and collaborators for post-mitotic aneuploid neurons in AD brains (Bajic et al., 2015; Arendt et al., 2015).

The presence of tau, non-phosphorylated at various epitopes, in AD and tauopathy brains, has long been underestimated until described by recent studies (Kimura et al., 2016; Lewczuk et al., 2017; Calderón-Garcidueñas et al., 2018). Likewise, our study highlights the unexpected implication of hypoP tau in the neuronal cell cycle process early during the development of AD. We cannot exclude that the lack of phosphorylation in AD brains might, at least partially, result from phosphatase activities during the post-mortem interval. Nevertheless, the existence of tau, non-phosphorylated at the epitope recognized by the Tau1 antibody, has previously been detected in neuronal nuclei in cellular and in vivo models as well as in control and AD human brains (Brady et al., 1995; Sultan et al., 2011; Violet et al., 2014; Ulrich et al., 2018). Only few epitopes of tau, such as serine 262, have been reported to exist in a phosphorylated state in neuronal nuclei (Sultan et al., 2011, Violet et al., 2014; Ulrich et al., 2018). Interestingly, besides its capacity to inhibit tau binding to microtubules and actin, phosphorylation of serine 262 can actively inhibit tau aggregation and seeding activity, suggesting properties to prevent the development of tau pathology (Haj-Yahya et al., 2020). However, the phosphorylation state of more tau epitopes should be investigated to disclose the full tau phosphorylation profile in ntau$^+$ cycling neurons. In addition, other post-translational modifications, such as tau acetylation, which was recently detected in the nucleus of cells in response to DNA damage, demand further analysis (Portillo et al., 2021).

We confirmed the presence of phosphorylated tau on DNA from mitotic neuroblastoma cells (SH-SY5Y) (Supplementary Fig. 11), which is in accordance with the detection of hyperphosphorylated tau in the cell cycle exclusively during mitosis in cancer cells and *Xenopus* laevis oocytes (Pope et al., 1994; Preuss et al., 1998; Illenberger et al., 1998; Delobel et al., 2002; Flores-Rodríguez et al., 2019). Therefore, the absence of tau hyperphosphorylation in ntau$^+$ neurons with increased DNA content derived from AD brain, which do not complete replication nor progress to mitosis, is in accordance with the results previously reported in proliferative cells during the G1 and S phases of the cell cycle. Notwithstanding the persistent activation of the cell cycle can favor the appearance of tau hyperphosphorylation in neurons in vitro (McShea et al., 2007), the observed absence of tau phosphorylation on various epitopes in ntau$^+$ cycling neurons suggests that this process is not, or at least not directly, involved in the progression of tau pathology in AD brains. Our results thus challenge the current view that neuronal cell cycle reactivation contributes to tau pathology in AD brains.

Since the amount of nuclear tau in ntau$^+$ cycling neurons is strongly correlated with the level of oxidized guanine (8oxoG) and the presence of nuclear tau has previously been linked to the DDR (Sultan et al., 2011; Violet et al., 2014; Mansuroglu et al., 2016; Bou Samra et al., 2017), we suggest that tau is recruited into the nucleus of cycling neurons in response to early oxidative DNA modification. In the recent past, a possible role for tau in the DNA repair process was proposed in neurons (Violet et al., 2015; Mansuroglu et al., 2016), however, the fact that repression of tau does not alter the level of 8oxoG in our observations, indicates the unlikeliness for tau to be involved in the oxidative DNA damage repair mechanism in ntau$^+$ cycling neurons from AD brains.

The presence of 8oxoG in the nucleus is mainly considered to represent deleterious DNA damage for the cell due to its mutagenic power. However, increasing evidence also shows a beneficial role of 8oxoG as an epigenetic mark capable of modulating gene transcription in response to oxidative stress (Fleming et al., 2017;Bokhari et al., 2019). Subsequently, it is tempting to hypothesize that the persistent presence of unrepaired oxidative damage in ntau$^+$ cycling neurons in AD brains reflects an epigenetic mechanism to adapt to a high rate of oxidative stress, by regulating gene transcription in order to preserve neuronal homeostasis and prevent cell death. Therefore, the recruitment of hypoP tau into the nucleus of neurons might occur in response to beneficial oxidative stress-induced epigenetic changes rather than deleterious damage in neuronal DNA from AD brains. This would explain why ntau$^+$ cycling neurons can survive despite a high level of 8oxoG.

The absence of a treatment to stop, or at least effectively slow down the progression of AD pathology urges the identification of new relevant therapeutic targets. Reducing tau in neurons has been proposed as potential strategies (Jadhav et al., 2019). However, this should be carefully evaluated as tau depletion could trigger an overload of neuronal DNA damage in the brain (Violet et al., 2014) and favor apoptosis. As a bold proposal, we propose that forcing the progression of the cell cycle might protect neurons residing in a toxic environment from cell death and prevent the strong neuronal loss observed in AD brains during the early stages of the pathology, thereby slowing down the progression of the disease. Of course, a first step should be to elucidate the underlying molecular mechanisms which control the tau-dependent cell cycle progress and to decipher pro-survival actors in AD brains which could be manipulated to prevent neuronal cell death.

5. Conclusions

We report for the first time a pro-survival role of tau triggering the

progression of the cell cycle in S phase in neurons. The unexpected synergy between hypoP tau and the cell cycle is likely part of an adaptive process to efficiently prevent oxidative stress-related neuronal cell death. Our results suggest a tau-dependent protective effect of neuronal cell cycle reactivation in AD brains, early during the development of the pathology, and challenge the current view that the neuronal cell cycle is an early mediator of AD pathology.

Ethics approval and consent to participate

Adult control and AD human brain samples were obtained from the Lille Neurobank (Lille, France), which was given to the French Research Ministry by the Lille Regional Hospital (CHRU-Lille) on August 14, 2008 under the reference DC- 2000–642. The Lille Neurobank fulfills criteria from the French Law on biological re-sources, including informed consent, ethics review committee, and data protection (article L1243–4 du Code de la Santé publique, August 2007). A selection of control brains for FACS analysis was obtained from the Neurobiobank of the Institute Born-Bunge (NBB-IBB; FAGG enlisted registration number BB190113) (University of Antwerp, Belgium). Ethical approval was obtained from the UZ Leuven (NH019–2018–09–01).

The animals were maintained in compliance with institutional protocols (Comité d'éthique en expérimentation animale du Nord Pas-de-Calais, n°0508003). All of the animal experiments were performed in compliance with and following the approval of the local Animal Ethical Committee (agreement #12787–2, 015, 101, 320, 441, 671 v9nfrom CEEA75, Lille, France), standards for the care and use of laboratory animals, and the French and European Community rules.

Consent for publication

Yes.

Funding

This work was supported by grants from the program Investisement d'avenir LabEx (Laboratory Excellence) DISTALZ (Development of Innovative Strategies for a Transdisciplinary approach to ALZheimer's disease). Our laboratories are also supported by LICEND (Lille Center of Excellence in Neurodegenerative Disorders), CNRS, Inserm, Métropole Européenne de Lille, Univ. Lille, FEDER and DN2M. M-C.G and B. D were also supported by INSTALZ, an EU Joint Programme - Neurodegenerative Disease Research (JPND) project. The INSTALZ project is supported through the following funding organisations under the aegis of JPND - "http://www. jpnd.eu" (Belgium, Research Foundation Flanders; Denmark, Innovation Fund Denmark; France, Agence Nationale de la Recherche; Sweden, Swedish Re- search Council; United Kingdom, Medical Research Council). The project has received funding from the European Union's Horizon 2020 research and innovation programme under grant agreement No 643417. B.D. is supported by an Odysseus type 1 Grant of the Research Foundation Flanders (3G0H8318), a starting grant from the Ghent University Special Research Fund (01N10319) and the Ghent University Fund for Alzheimer's Disease and Related Disorders. SG is supported by a Ph.D. fellowship of The Research Foundation – Flanders (FWO, 1S24019N).

CRediT authorship contribution statement

MD, SG, TC, SB, AGN, LAP, TB, MV, SV, MCG performed experiments and analyzed data. EB, BL and TV discussed results. YV, PPDD, RP, VD, CAM provided human brain samples and discussed results. ND designed and provided the LV-shctrl and discussed results. MC designed and provided the LV-shtau, and discussed the results. MCG and BD designed the project, analyzed the data, and prepared the manuscript. LB discussed the results and helped with writing the manuscript. MCG and BD supervised the project. All authors read and approved the final manuscript.

Declaration of Competing Interests

The authors declare that they have no competing interests.

Data availability

No data was used for the research described in the article.

Acknowledgments

This article is dedicated to Pr. Charles Duyckaerts (2022.08.06). We are grateful to the IMPRT (Institut de Médecine Prédictive et de Recherche Thérapeutique, Lille, France) for access to the confocal microscopy platform and the animal facility. We are grateful to M. Tardivel and A. Bongiovanni for their assistance with confocal microscopy analyses, and to M.H. Gevaert (Laboratoire d'Histologie, Faculté de Médecine, Lille) and Raphaëlle Caillierez for technical assistance. We thank Ariane Sharif for her advice about BrdU incorporation. Many thanks to Piet Rodriguez for his help in the realization of the graphical summary. We express our gratitude to Alzheimer's patients and their families for accepting autopsies and the use of post mortem brain material for research.

Appendix A. Supporting information

Supplementary data associated with this article can be found in the online version at doi:10.1016/j.pneurobio.2022.102386.

References

Andorfer, C., Acker, C.M., Kress, Y., Hof, P.R., Duff, K., Davies, P., 2005. Cell-cycle reentry and cell death in transgenic mice expressing nonmutant human tau isoforms. J. Neurosci. 25, 5446–5454. https://doi.org/10.1523/JNEUROSCI.4637-04.2005.

Aranda-Anzaldo, A., Dent, M.A., 2017. Why cortical neurons cannot divide, and why do they usually die in the attempt? J. Neurosci. Res. 95, 921–929. https://doi.org/10.1002/jnr.23765.

Arendt, T., 2000. Alzheimer's disease as a loss of differentiation control in a subset of neurons that retain immature features in the adult brain. Neurobiol. Aging 21, 783–796. https://doi.org/10.1016/s0197-4580(00)00216-5.

Arendt, T., 2012. Cell cycle activation and aneuploid neurons in Alzheimer's disease. Mol. Neurobiol. 46, 125–135. https://doi.org/10.1007/s12035-012-8262-0.

Arendt, T., Mosch, B., Morawski, M., 2009. Neuronal aneuploidy in health and disease: a cytomic approach to understand the molecular individuality of neurons. Int. J. Mol. Sci. 10, 1609–1627. https://doi.org/10.3390/ijms10041609.

Arendt, T., Brückner, M.K., Lösche, A., 2015. Regional mosaic genomic heterogeneity in the elderly and in Alzheimer's disease as a correlate of neuronal vulnerability. Acta Neuropathol. 130, 501–510. https://doi.org/10.1007/s00401-015-1465-5.

Arendt, T., Holzer, M., Grossmann, A., Zedlick, D., Brückner, M.K., 1995. Increased expression and subcellular translocation of the mitogen activated protein kinase kinase and mitogen-activated protein kinase in Alzheimer's disease. Neuroscience 68, 5–18. https://doi.org/10.1016/0306-4522(95)00146-a.

Bajic, V., Spremo-Potparevic, B., Zivkovic, L., Isenovic, E.R., Arendt, T., 2015. Cohesion and the aneuploid phenotype in Alzheimer's disease: a tale of genome instability. Neurosci. Biobehav. Rev. 55, 365–374. https://doi.org/10.1016/j.neubiorev.2015.05.010.

Bokhari, B., Sharma, S., 2019. Stress marks on the genome: use or lose. Int. J. Mol. Sci. 20, 364. https://doi.org/10.3390/ijms20020364.

Bonda, D.J., Evans, T.A., Santocanale, C., Llosá, J.C., Viña, J., Bajic, V., Castellani, R.J., Siedlak, S.L., Perry, G., Smith, M.A., Lee, H.G., 2009. Evidence for the progression through S-phase in the ectopic cell cycle re-entry of neurons in Alzheimer disease. Aging 1, 382–388. https://doi.org/10.18632/aging.100044.

Bou Samra, E., Buhagiar-Labarchède, G., Machon, C., Guitton, J., Onclercq-Delic, R., Green, M.R., Alibert, O., Gazin, C., Veaute, X., Amor-Guéret, M., 2017. A role for Tau protein in maintaining ribosomal DNA stability and cytidine deaminase-deficient cell survival. Nat. Commun. 8, 693. https://doi.org/10.1038/s41467-017-00633-1.

Bougé, A.L., Parmentier, M.L., 2016. Tau excess impairs mitosis and kinesin-5 function, leading to aneuploidy and cell death. Dis. Model Mech. 9, 307–319. https://doi.org/10.1242/dmm.022558.

Brady, R.M., Zinkowski, R.P., Binder, L.I., 1995. Presence of tau in isolated nuclei from human brain. Neurobiol. Aging 16, 479–486. https://doi.org/10.1016/0197-4580(95)00023-8.

Buée-Scherrer, V., Condamines, O., Mourton-Gilles, C., Jakes, R., Goedert, M., Pau, B., Delacourte, A., 1996. AD2, a phosphorylation-dependent monoclonal antibody directed against tau proteins found in Alzheimer's disease. Brain Res. Mol. Brain Res. 39, 79–88. https://doi.org/10.1016/0169-328x(96)00003-4.

Bushman, D.M., Kaeser, G.E., Siddoway, B., Westra, J.W., Rivera, R.R., Rehen, S.K., Yung, Y.C., Chun, J., 2015. Genomic mosaicism with increased amyloid precursor

protein (APP) gene copy number in single neurons from sporadic Alzheimer's disease brains. eLife 4, e05116. https://doi.org/10.7554/eLife.05116.
Busser, J., Geldmacher, D.S., Herrup, K., 1998. Ectopic cell cycle proteins predict the sites of neuronal cell death in Alzheimer's disease brain. J. Neurosci. 182801–182807. https://doi.org/10.1523/JNEUROSCI.18-08-02801.
Cai, X., Evrony, G.D., Lehmann, H.S., Elhosary, P.C., Mehta, B.K., Poduri, A., Walsh, C.A., 2014. Single-cell, genome-wide sequencing identifies clonal somatic copy-number variation in the human brain. Cell Rep. 8, 1280–1289. https://doi.org/10.1016/j.celrep.2014.07.043.
Calderón-Garcidueñas, L., Mukherjee, P.S., Waniek, K., Holzer, M., Chao, C.K., Thompson, C., Ruiz-Ramos, R., Calderón-Garcidueñas, A., Franco-Lira, M., Reynoso-Robles, R., Gónzalez-Maciel, A., Lachmann, I., 2018. Non-phosphorylated Tau in cerebrospinal fluid is a marker of Alzheimer's disease continuum in young urbanites exposed to air pollution. J. Alzheimers Dis. 66, 1437–1451. https://doi.org/10.3233/JAD-180853.
Cioffi, F., Adam, R.H.I., Broersen, K., 2019. Molecular mechanisms and genetics of oxidative stress in Alzheimer's disease. J. Alzheimers Dis. 72, 981–1017. https://doi.org/10.3233/JAD-190863.
Costantino, I., Nicodemus, J., Chun, J., 2021. Genomic mosaicism formed by somatic variation in the aging and diseased brain. Genes 12, 1071. https://doi.org/10.3390/genes12071071.
Delobel, P., Flament, S., Hamdane, M., Mailliot, C., Sambo, A.V., Bégard, S., Sergeant, N., Delacourte, A., Vilain, J.P., Buée, L., 2002. Abnormal Tau phosphorylation of the Alzheimer-type also occurs during mitosis. J. Neurochem. 83, 412–420. https://doi.org/10.1046/j.1471-4159.2002.01143.
van den Bos, H., Spierings, D.C., Taudt, A.S., Bakker, B., Porubský, D., Falconer, E., Novoa, C., Halsema, N., Kazemier, H.G., Hoekstra-Wakker, K., Guryev, V., den Dunnen, W.F., Foijer, F., Tatché, M.C., Boddeke, H.W., Lansdorp, P.M., 2016. Single-cell whole genome sequencing reveals no evidence for common aneuploidy in normal and Alzheimer's disease neurons. Genome Biol. 17, 116. https://doi.org/10.1186/s13059-016-0976-2.
Dourlen, P., Ando, K., Hamdane, M., Begard, S., Buée, L., Galas, M.C., 2007. The peptidyl prolyl cis/trans isomerase Pin1 downregulates the Inhibitor of Apoptosis Protein Survivin. Biochim. Biophys. Acta 1773, 1428–1437. https://doi.org/10.1016/j.bbamcr.2007.05.012.
Dull, T., Zufferey, R., Kelly, M., Mandel, R.J., Nguyen, M., Trono, D., Naldini, L., 1998. A third-generation lentivirus vector with a conditional packaging system. J. Virol. 72, 8463–8471. https://doi.org/10.1128/JVI.72.11.8463-8471.1998.
Fischer, H.G., Morawski, M., Brückner, M.K., Mittag, A., Tarnok, A., Arendt, T., 2012. Changes in neuronal DNA content variation in the human brain during aging. Aging Cell 11, 628–633. https://doi.org/10.1111/j.1474-9726.2012.00826.
Fleming, A.M., Burrows, C.J., 2017. 8-Oxo-7,8-dihydroguanine, friend and foe: epigenetic-like regulator versus initiator of mutagenesis. DNA Repair 75–83. https://doi.org/10.1016/j.dnarep.2017.06.009.
Flores-Rodríguez, P., Harrington, C.R., Wischik, C.M., Ibarra-Bracamontes, V., Zarco, N., Navarrete, A., Martínez-Maldonado, A., Guadarrama-Ortíz, P., Villanueva-Fierro, I., Ontiveros-Torres, M.A., Perry, G., Alonso, A.D., Floran-Garduño, B., Segovia, J., Luna-Muñoz, J., 2019. Phospho-tau protein expression in the cell cycle of SH-SY5Y neuroblastoma cells: a morphological study. J. Alzheimers Dis. 71, 631–645. https://doi.org/10.3233/JAD-190155.
Galas, M.C., Dourlen, P., Bégard, S., Ando, K., Blum, D., Hamdane, M., Buée, L., 2006. The peptidylprolyl cis/trans-isomerase Pin1 modulates stress-induced dephosphorylation of Tau in neurons. Implication in a pathological mechanism related to Alzheimer disease. J. Biol. Chem. 281, 19296–19304. https://doi.org/10.1074/jbc.M601849200.
Gao, Z., Fu, H.J., Zhao, L.B., Sun, Z.Y., Yang, Y.F., Zhu, H.Y., 2018. Aberrant DNA methylation associated with Alzheimer's disease in the superior temporal gyrus. Exp. Ther. Med. 15, 103–108. https://doi.org/10.3892/etm.2017.5394.
Haj-Yahya, M., Gopinath, P., Rajasekhar, K., Mirbaha, H., Diamond, M.I., Lashuel, H.A., 2020. Site-specific hyperphosphorylation inhibits, rather than promotes, tau fibrillization, seeding capacity, and its microtubule binding. Angew. Chem. Int. Ed. 59, 4059–4067. https://doi.org/10.1002/anie.201913001.
Herrup, K., Neve, R., Ackerman, S.L., Copani, A., 2004. Divide and die: cell cycle events as triggers of nerve cell death. J. Neurosci. 24, 9232–9239. https://doi.org/10.1523/JNEUROSCI.3347-04.2004.
Hoozemans, J.J., Brückner, M.K., Rozemuller, A.J., Veerhuis, R., Eikelenboom, P., Arendt, T., 2002. Cyclin D1 and cyclin E are co-localized with cyclo-oxygenase 2 (COX-2) in pyramidal neurons in Alzheimer disease temporal cortex. J. Neuropathol. Exp. Neurol. 61, 678–688. https://doi.org/10.1093/jnen/61.8.678.
Hottinger, A.F., Azzouz, M., Déglon, N., Aebischer, P., Zurn, A.D., 2000. Complete and long-term rescue of lesioned adult motoneurons by lentiviral-mediated expression of glial cell line-derived neurotrophic factor in the facial nucleus. J. Neurosci. 20, 5587–5593. https://doi.org/10.1523/JNEUROSCI.20-15-05587.2000.
Hradek, A.C., Lee, H.P., Siedlak, S.L., Torres, S.L., Jung, W., Han, A.H., Lee, H.G., 2015. Distinct chronology of neuronal cell cycle re-entry and tau pathology in the 3xTg-AD mouse model and Alzheimer's disease patients. J. Alzheimers Dis. 43, 57–65. https://doi.org/10.3233/JAD-141083.
Huang, F., Wang, M., Liu, R., Wang, J.Z., Schadt, E., Haroutunian, V., Katsel, P., Zhang, B., Wang, X., 2019. CDT2-controlled cell cycle reentry regulates the pathogenesis of Alzheimer's disease. Alzheimers Dement. 15, 217–231. https://doi.org/10.1016/j.jalz.2018.08.013.
Illenberger, S., Zheng-Fischhöfer, Q., Preuss, U., Stamer, K., Baumann, K., Trinczek, B., Biernat, J., Godemann, R., Mandelkow, E.M., Mandelkow, E., 1998. The endogenous and cell cycle-dependent phosphorylation of tau protein in living cells: implications for Alzheimer's disease. Mol. Biol. Cell 9, 1495–1512. https://doi.org/10.1091/mbc.9.6.1495.
Ippati, S., Deng, Y., van der Hoven, J., Heu, C., van Hummel, A., Chua, S.W., Paric, E., Chan, G., Feiten, A., Fath, T., Ke, Y.D., Haass, N.K., Ittner, L.M., 2021. Rapid initiation of cell cycle reentry processes protects neurons from amyloid-β toxicity. Proc. Natl. Acad. Sci. USA 118, e2011876118. https://doi.org/10.1073/pnas.2011876118.
Jadhav, S., Avila, J., Schöll, M., Kovacs, G.G., Kövari, E., Skrabana, R., Evans, L.D., Kontsekova, E., Malawska, B., de Silva, R., Buee, L., Zilka, N., 2019. A walk through tau therapeutic strategies. Acta Neuropathol. Commun. 27, 22. https://doi.org/10.1186/s40478-019-0664-z.
Johansson, A., Hampel, H., Faltraco, F., Buerger, K., Minthon, L., Bogdanovic, N., Sjögren, M., Zetterberg, H., Forsell, L., Lilius, L., Wahlund, L.O., Rymo, L., Prince, J. A., Blennow, K., 2003. Increased frequency of a new polymorphism in the cell division cycle 2 (cdc2) gene in patients with Alzheimer's disease and frontotemporal dementia. Neurosci. Lett. 340 (1), 69–73. https://doi.org/10.1016/s0304-3940(03)00051-x.
Joseph, C., Mangani, A.S., Gupta, V., Chitranshi, N., Shen, T., Dheer, Y., Kb, D., Mirzaei, M., You, Y., Graham, S.L., Gupta, V., 2020. Cell cycle deficits in neurodegenerative disorders: uncovering molecular mechanisms to drive innovative therapeutic development. Aging Dis. 11, 946–966. https://doi.org/10.14336/AD.2019.0923.
Kagias, K., Nehammer, C., Pocock, R., 2012. Neuronal responses to physiological stress. Front Genet. 3, 222. https://doi.org/10.3389/fgene.2012.00222.
Kamada, S., Kikkawa, U., Tsujimoto, Y., Hunter, T., 2005. Nuclear translocation of caspase-3 is dependent on its proteolytic activation and recognition of a substrate-like protein(s). J. Biol. Chem. 280, 857–860. https://doi.org/10.1074/jbc.C400538200.
Khurana, V., Lu, Y., Steinhilb, M.L., Oldham, S., Shulman, J.M., Feany, M.B., 2006. TOR-mediated cell-cycle activation causes neurodegeneration in a Drosophila tauopathy model. Curr. Biol. 16, 230–241. https://doi.org/10.1016/j.cub.2005.12.042.
Kimura, T., Hatsuta, H., Masuda-Suzukake, M., Hosokawa, M., Ishiguro, K., Akiyama, H., Murayama, S., Hasegawa, M., Hisanaga, S., 2016. The abundance of nonphosphorylated Tau in mouse and human tauopathy brains revealed by the use of phos-Tag method. Am. J. Pathol. 186, 398–409. https://doi.org/10.1016/j.ajpath.2015.10.009.
Klein, J.A., Ackerman, S.L., 2003. Oxidative stress, cell cycle, and neurodegeneration. J. Clin. Investig. 111, 785–793. https://doi.org/10.1172/JCI18182.
Kruman, I.I., Wersto, R.P., Cardozo-Pelaez, F., Smilenov, L., Chan, S.L., Chrest, F.J., Emokpae Jr, R., Gorospe, M., Mattson, M.P., 2004. Cell cycle activation linked to neuronal cell death initiated by DNA damage. Neuron 41, 549–561. https://doi.org/10.1016/s0896-6273(04)00017-0.
Lewczuk, P., Lelental, N., Lachmann, I., Holzer, M., Flach, K., Brandner, S., Engelborghs, S., Teunissen, C.E., Zetterberg, H., Molinuevo, J.L., Mroczko, B., Blennow, K., Popp, J., Parnetti, L., Chiasserini, D., Perret-Liaudet, A., Spitzer, P., Maler, J.M., Kornhuber, J., 2017. Non-phosphorylated Tau as a potential biomarker of Alzheimer's disease: analytical and diagnostic characterization. J. Alzheimers Dis. 55, 159–170. https://doi.org/10.3233/JAD-160448.
Li, H., 2013. Aligning sequence reads, clone sequences and assembly contigs with BWA-MEM. arXiv 1303, 3997. ⟨https://arxiv.org/abs/1303.3997⟩.
Lodato, M.A., Woodworth, M.B., Lee, S., Evrony, G.D., Mehta, B.K., Karger, A., Lee, S., Chittenden, T.W., D'Gama, A.M., Cai, X., Luquette, L.J., Lee, E., Park, P.J., Walsh, C. A., 2015. Somatic mutation in single human neurons tracks developmental and transcriptional history. Science 350, 94–98. https://doi.org/10.1126/science.aab1785.
López-Sánchez, N., Fontán-Lozano, Á., Pallé, A., González-Álvarez, V., Rábano, A., Trejo, J.L., Frade, J.M., 2017. Neuronal tetraploidization in the cerebral cortex correlates with reduced cognition in mice and precedes and recapitulates Alzheimer's-associated neuropathology. Neurobiol. Aging 56, 50–66. https://doi.org/10.1016/j.neurobiolaging.2017.04.008.
Ma, H., Dong, Y., Chu, Y., Guo, Y., Li, L., 2022. The mechanisms of ferroptosis and its role in alzheimer's disease. Front. Mol. Biosci. 9, 965064 https://doi.org/10.3389/fmolb.2022.965064.
Macaulay, I.C., Teng, M.J., Haerty, W., Kumar, P., Ponting, C.P., Voet, T., 2016. Separation and parallel sequencing of the genomes and transcriptomes of single cells using G&T-seq. Nat. Protoc. 11, 2081–2103. https://doi.org/10.1038/nprot.2016.138.
Macaulay, I.C., Haerty, W., Kumar, P., Li, Y.I., Hu, T.X., Teng, M.J., Goolam, M., Saurat, N., Coupland, P., Shirley, L.M., Smith, M., Van der Aa, N., Banerjee, R., Ellis, P.D., Quail, M.A., Swerdlow, H.P., Zernicka-Goetz, M., Livesey, F.J., Ponting, C. P., Voet, T., 2015. G&T-seq: parallel sequencing of single-cell genomes and transcriptomes. Nat. Methods 12, 519–522. https://doi.org/10.1038/nmeth.3370.
Maher, P., Currais, A., Schubert, D., 2020. Using the oxytosis/ferroptosis pathway to understand and treat age-associated neurodegenerative diseases. Cell Chem. Biol. 27, 1456–1471. https://doi.org/10.1016/j.chembiol.2020.10.010.
Malmanche, N., Dourlen, P., Gistelinck, M., Demiautte, F., Link, N., Dupont, C., Vanden Broeck, L., Werkmeister, E., Amouyel, P., Bongiovanni, A., Bauderlique, H., Moechars, D., Royou, A., Bellen, H.J., Lafont, F., Callaerts, P., Lambert, J.C., Dermaut, B., 2017. Developmental expression of 4-repeat-Tau induces neuronal aneuploidy in drosophila tauopathy models. Sci. Rep. 7, 40764. https://doi.org/10.1038/srep40764.
Mansuroglu, Z., Benhelli-Mokrani, H., Marcato, V., Sultan, A., Violet, M., Chauderlier, A., Delattre, L., Loyens, A., Talahari, S., Bégard, S., Nesslany, F., Colin, M., Souès, S., Lefebvre, B., Buée, L., Galas, M.C., Bonnefoy, E., 2016. Loss of Tau protein affects the structure, transcription and repair of neuronal pericentromeric heterochromatin. Sci. Rep. 6, 33047 https://doi.org/10.1038/srep33047.
Martellucci, S., Clementi, L., Sabetta, S., Muzi, P., Mattei, V., Bologna, M., Angelucci, A., 2021. Tau oligomers accumulation sensitizes prostate cancer cells to docetaxel

treatment. J. Cancer Res. Clin. Oncol. 147, 1957–1971. https://doi.org/10.1007/s00432-021-03598-3.
McConnell, M.J., Lindberg, M.R., Brennand, K.J., Piper, J.C., Voet, T., Cowing-Zitron, C., Shumilina, S., Lasken, R.S., Vermeesch, J.R., Hall, I.M., Gage, F.H., 2013. Mosaic copy number variation in human neurons. Science 342, 632–637. https://doi.org/10.1126/science.1243472.
McShea, A., Lee, H.G., Petersen, R.B., Casadesus, G., Vincent, I., Linford, N.J., Funk, J.O., Shapiro, R.A., Smith, M.A., 2007. Neuronal cell cycle re-entry mediates Alzheimer disease-type changes. Biochim. Biophys. Acta 772, 467–472. https://doi.org/10.1016/j.bbadis.2006.09.010.
Miller, I., Min, M., Yang, C., Tian, C., Gookin, S., Carter, D., Spencer, S.L., 2018. Ki67 is a graded rather than a binary marker of proliferation versus quiescence. Cell Rep. 24 (1105–1112), e5 https://doi.org/10.1016/j.celrep.2018.06.110.
Mosch, B., Morawski, M., Mittag, A., Lenz, D., Tarnok, A., Arendt, T., 2007. Aneuploidy and DNA replication in the normal human brain and Alzheimer's disease. J. Neurosci. 27, 6859–6867. https://doi.org/10.1523/JNEUROSCI.0379-07.2007.
Nagy, Z., Esiri, M.M., Smith, A.D., 1997. Expression of cell division markers in the hippocampus in Alzheimer's disease and other neurodegenerative conditions. Acta Neuropathol. 93, 294–300. https://doi.org/10.1007/s004010050617.
Nandakumar, S., Rozich, E., Buttitta, L., 2021. Cell cycle re-entry in the nervous system: from polyploidy to neurodegeneration. Front. Cell Dev. Biol. 9, 698661 https://doi.org/10.3389/fcell.2021.698661.
Nobuhara, C.K., DeVos, S.L., Commins, C., Wegmann, S., Moore, B.D., Roe, A.D., Costantino, I., Frosch, M.P., Pitstick, R., Carlson, G.A., Hock, C., Nitsch, R.M., Montrasio, F., Grimm, J., Cheung, A.E., Dunah, A.W., Wittmann, M., Bussiere, T., Weinreb, P.H., Hyman, B.T., Takeda, S., 2017. Tau antibody targeting pathological species blocks neuronal uptake and interneuron propagation of Tau in vitro. Am. J. Pathol. 187, 1399–1412. https://doi.org/10.1016/j.ajpath.2017.01.022.
Park, K.H., Hallows, J.L., Chakrabarty, P., Davies, P., Vincent, I., 2007. Conditional neuronal simian virus 40 T antigen expression induces Alzheimer-like tau and amyloid pathology in mice. J. Neurosci. 27, 2969–2978. https://doi.org/10.1523/JNEUROSCI.0186-07.2007.
Pei, J.J., Braak, H., Gong, C.X., Grundke-Iqbal, I., Iqbal, K., Winblad, B., Cowburn, R.F., 2002. Up-regulation of cell division cycle (cdc) 2 kinase in neurons with early stage Alzheimer's disease neurofibrillary degeneration. Acta Neuropathol. 104, 369–376. https://doi.org/10.1007/s00401-002-0565-1.
Pensalfini, A., Albay 3rd, R., Rasool, S., Wu, J.W., Hatami, A., Arai, H., Margol, L., Milton, S., Poon, W.W., Corrada, M.M., Kawas, C.H., Glabe, C.G., 2014. Intracellular amyloid and the neuronal origin of Alzheimer neuritic plaques. Neurobiol. Dis. 71, 53–61. https://doi.org/10.1016/j.nbd.2014.07.011.
Pope, W.B., Lambert, M.P., Leypold, B., Seupaul, R., Sletten, L., Krafft, G., Klein, W.L., 1994. Microtubule-associated protein tau is hyperphosphorylated during mitosis in the human neuroblastoma cell line SH-SY5Y. Exp. Neurol. 126, 185–194. https://doi.org/10.1006/exnr.1994.1057.
Portillo, M., Eremenko, E., Kaluski, S., Garcia-Venzor, A., Onn, L., Stein, D., Slobodnik, Z., Zaretsky, A., Ueberham, U., Einav, M., Brückner, M.K., Arendt, T., Toiber, D., 2021. SIRT6-CBP-dependent nuclear Tau accumulation and its role in protein synthesis. Cell Rep. 35, 109035 https://doi.org/10.1016/j.celrep.2021.109035.
Potter, H., Chial, H.J., Caneus, J., Elos, M., Elder, N., Borysov, S., Granic, A., 2019. Chromosome instability and mosaic aneuploidy in neurodegenerative and neurodevelopmental disorders. Front. Genet. 10, 1092. https://doi.org/10.3389/fgene.2019.01092.
Preuss, U., Mandelkow, E.M., 1998. Mitotic phosphorylation of tau protein in neuronal cell lines resembles phosphorylation in Alzheimer's disease. Eur. J. Cell Biol. 76, 176–184. https://doi.org/10.1016/S0171-9335(98)80032-0.
Rohrback, S., Siddoway, B., Liu, C.S., Chun, J., 2018. Genomic mosaicism in the developing and adult brain. Dev. Neurobiol. 78, 1026–1048. https://doi.org/10.1002/dneu.22626.
Rossi, G., Conconi, D., Panzeri, E., Redaelli, S., Piccoli, E., Paoletta, L., Dalprà, L., Tagliavini, F., 2013. Mutations in MAPT gene cause chromosome instability and introduce copy number variations widely in the genome. J. Alzheimers Dis. 33, 969–982. https://doi.org/10.3233/JAD-2012-121633.
Rossi, G., Dalprà, L., Crosti, F., Lissoni, S., Sciacca, F.L., Catania, M., Di Fede, G., Mangieri, M., Giaccone, G., Croci, D., Tagliavini, F., 2008. A new function of microtubule-associated protein tau: involvement in chromosome stability. Cell Cycle 7, 1788–1794. https://doi.org/10.4161/cc.7.12.6012.
Schindowski, K., Belarbi, K., Bretteville, A., Ando, K., Buée, L., 2008. Neurogenesis and cell cycle-reactivated neuronal death during pathogenic tau aggregation. Genes Brain Behav. 7 (Suppl 1(1)), 92–100. https://doi.org/10.1111/j.1601-183X.2007.00377.
Schwartz, E.I., Smilenov, L.B., Price, M.A., Osredkar, T., Baker, R.A., Ghosh, S., Shi, F.D., Vollmer, T.L., Lencinas, A., Stearns, D.M., Gorospe, M., Kruman, I.I., 2007. Cell cycle activation in postmitotic neurons is essential for DNA repair. Cell Cycle 6, 318–329. https://doi.org/10.4161/cc.6.3.3752.
Seward, M.E., Swanson, E., Norambuena, A., Reimann, A., Cochran, J.N., Li, R., Roberson, E.D., Bloom, G.S., 2013. Amyloid-β signals through tau to drive ectopic neuronal cell cycle re-entry in Alzheimer's disease. J. Cell Sci. 126, 1278–1286. https://doi.org/10.1242/jcs.1125880.
Shanbhag, N.M., Evans, M.D., Mao, W., Nana, A.L., Seeley, W.W., Adame, A., Rissman, R.A., Masliah, E., Mucke, L., 2019. Early neuronal accumulation of DNA double strand breaks in Alzheimer's disease. Acta Neuropathol. Commun. 7, 77. https://doi.org/10.1186/s40478-019-0723-5.
Shepherd, C.E., Yang, Y., Halliday, G.M., 2018. Region- and cell-specific aneuploidy in brain aging and neurodegeneration. Neuroscience 374, 326–334. https://doi.org/10.1016/j.neuroscience.2018.01.050.
Smith, T.W., Lippa, C.F., 1995. Ki-67 immunoreactivity in Alzheimer's disease and other neurodegenerative disorders. J. Neuropathol. Exp. Neurol. 54, 297–303. https://doi.org/10.1097/00005072-199505000-00002.
Stone, J.G., Siedlak, S.L., Tabaton, M., Hirano, A., Castellani, R.J., Santocanale, C., Perry, G., Smith, M.A., Zhu, X., Lee, H.G., 2011. The cell cycle regulator phosphorylated retinoblastoma protein is associated with tau pathology in several tauopathies. J. Neuropathol. Exp. Neurol. 70, 578–587. https://doi.org/10.1097/NEN.0b013e3182204414.
Sultan, A., Nesslany, F., Violet, M., Bégard, S., Loyens, A., Talahari, S., Mansuroglu, Z., Marzin, D., Sergeant, N., Humez, S., Colin, M., Bonnefoy, E., Buée, L., Galas, M.C., 2011. Nuclear tau, a key player in neuronal DNA protection. J. Biol. Chem. 286, 4566–4575. https://doi.org/10.1074/jbc.M110.199976.
Sun, X., Kaufman, P.D., 2018. Ki-67: more than a proliferation marker. Chromosoma 127, 175–186. https://doi.org/10.1007/s00412-018-0659-8.
Swiech, L., Heidenreich, M., Banerjee, A., Habib, N., Li, Y., Trombetta, J., Sur, M., Zhang, F., 2015. In vivo interrogation of gene function in the mammalian brain using CRISPR-Cas9. Nat. Biotechnol. 33, 102–106. https://doi.org/10.1038/nbt.3055.
Swomley, A.M., Förster, S., Keeney, J.T., Triplett, J., Zhang, Z., Sultana, R., Butterfield, D.A., 2014. Abeta, oxidative stress in Alzheimer disease: evidence based on proteomics studies. Biochim. Biophys. Acta 1842, 1248–1257. https://doi.org/10.1016/j.bbadis.2013.09.015.
Ulrich, G., Salvadè, A., Boersema, P., Calì, T., Foglieni, C., Sola, M., Picotti, P., Papin, S., Paganetti, P., 2018. Phosphorylation of nuclear Tau is modulated by distinct cellular pathways. Sci. Rep. 8, 17702 https://doi.org/10.1038/s41598-018-36374-4.
Van der Aa, N., Cheng, J., Mateiu, L., Zamani Esteki, M., Kumar, P., Dimitriadou, E., Vanneste, E., Moreau, Y., Vermeesch, J.R., Voet, T., 2013. Genome-wide copy number profiling of single cells in S-phase reveals DNA-replication domains. Nucleic Acids Res. 41, e66 https://doi.org/10.1093/nar/gks1352.
Violet, M., Delattre, L., Tardivel, M., Sultan, A., Chauderlier, A., Caillierez, R., Talahari, S., Nesslany, F., Lefebvre, B., Bonnefoy, E., Buée, L., Galas, M.C., 2014. A major role for Tau in neuronal DNA and RNA protection in vivo under physiological and hyperthermic conditions. Front. Cell Neurosci. 8, 84. https://doi.org/10.3389/fncel.2014.00084.
Violet, M., Chauderlier, A., Delattre, L., Tardivel, M., Chouala, M.S., Sultan, A., Marciniak, E., Humez, S., Binder, L., Kayed, R., Lefebvre, B., Bonnefoy, E., Buée, L., Galas, M.C., 2015. Prefibrillar Tau oligomers alter the nucleic acid protective function of Tau in hippocampal neurons in vivo. Neurobiol. Dis. 82, 540–551. https://doi.org/10.1016/j.nbd.2015.09.003.
Wartiovaara, K., Barnabe-Heider, F., Miller, F.D., Kaplan, D.R., 2002. N-myc promotes survival and induces S-phase entry of postmitotic sympathetic neurons. J. Neurosci. 22, 815–824. https://doi.org/10.1523/JNEUROSCI.22-03-00815.2002.
Westra, J.W., Barral, S., Chun, J., 2009. A reevaluation of tetraploidy in the Alzheimer's disease brain. Neurodegener. Dis. 6, 221–229. https://doi.org/10.1159/000236901.
Yang, Y., Mufson, E.J., Herrup, K., 2003. Neuronal cell death is preceded by cell cycle events at all stages of Alzheimer's disease. J. Neurosci. 23, 2557–2563. https://doi.org/10.1523/JNEUROSCI.23-07-02557.
Zheng, J., Akbari, M., Schirmer, C., Reynaert, M.L., Loyens, A., Lefebvre, B., Buée, L., Croteau, D.L., Galas, M.C., Bohr, V.A., 2020. Hippocampal tau oligomerization early in tau pathology coincides with a transient alteration of mitochondrial homeostasis and DNA repair in a mouse model of tauopathy. Acta Neuropathol. Commun. 8, 25. https://doi.org/10.1186/s40478-020-00896-8.
Zhu, X., McShea, A., Harris, P.L., Raina, A.K., Castellani, R.J., Funk, J.O., Shah, S., Atwood, C., Bowen, R., Bowser, R., Morelli, L., Perry, G., Smith, M.A., 2004. Elevated expression of a regulator of the G2/M phase of the cell cycle, neuronal CIP-1-associated regulator of cyclin B, in Alzheimer's disease. J. Neurosci. Res. 75, 698–703. https://doi.org/10.1002/jnr.20028.